Interim Progress Report on NASA Grant NAG5-2232

"Receiver Design, Performance Analysis, and Evaluation for Space-Borne Laser Altimeters and Space-to-Space Laser Ranging Systems"

for the period of April 15 1994 to October 15, 1994

Frederic M. Davidson
Xiaoli Sun
Christopher T. Field

October 1994

Department of Electrical and Computer Engineering
The Johns Hopkins University, Baltimore, MD 21218-2686

SUMMARY

This Interim report consists of two reports: "Space Radiation Effects on Si APDs for GLAS" and "Computer Simulation of Avalanche Photodiode and Preamplifier Output for Laser Altimeters." The former contains a detailed description of our proton radiation test of Si APDs performed at the Brookhaven National Laboratory. The latter documents the computer program subroutines which we wrote for the upgrade of NASA's GLAS simulator.

Space Radiation Effects on Si APDs for GLAS

Xiaoli Sun *
Daniel Reusser †

August 1994

Abstract

The test results are reported of proton radiation damage of Si APDs for use in the GLAS laser altimeter and the cloud lidar. The APD bulk leakage current increased at 0.26 fA/rad, or about 1600 dark counts/s per rad at $-10°C$ under 16.2 MeV protons. The space radiation damage is expected to cause the altimeter receiver noise spectral density to double after 3 krad at the end of the mission. The radiation damage to the Si APD single photon counter for the GLAS cloud lidar is expected to be much more severe and the receiver performance will be seriously affected, especially during nighttime operation.

*Department of ECE, the Johns Hopkins University
†USRA and Swiss National Science Foundation

1 Introduction

The Geoscience Laser Altimeter System (GLAS) consists of a laser altimeter at 1064 nm wavelength and a cloud lidar at 532 nm wavelength. A Si avalanche photodiode (APD) will be used as the altimeter photodetector. A photomultiplier tube or a Geiger mode Si APD single photon counter is currently being considered as the cloud lidar photodetector. It is estimated that GLAS will accumulate about 3 to 4 krad of space radiation over the 5 year mission with 7 mm thick aluminum shielding [1]. The type of radiations are primarily protons in the South Atlantic Anomaly and solar protons at the poles of the earth geomagnitosphere [2]. The energy spectrum of the protons is centered at about 50 MeV and extends from 1 MeV to several hundred MeV. We recently measured proton radiation damages of Si APDs for the GLAS mission. The results shows that Si APDs in linear mode for the GLAS altimeter will suffer significant but tolerable radiation damage after 3 krad total dose. However, Si APDs in Geiger mode as single photon counters are shown to suffer significant damages after as little as 100 rad and started to saturate after 3 krad at $-10°C$, and 200 rad at room temperature.

Due to their mass and charge, protons cause both ionization damages to the surface insulator layer and displacement damages to the crystal lattice in semiconductor devices [3]. Ionization damage is the major concern for surface devices, such as MOSFETs and CCDs. Displacement damage effectively adds defects to the semiconductor material and causes degradations in the device characteristics which are critically dependent on the number of defects in the material. Ionization damage is often tested with gamma rays because they are easy to obtain and has the same effects with respect to ionization damage. Displacement damage is often tested with neutrons which mainly cause displacement damage. Raymond and et al. showed that 1 rad of 1-100 MeV protons are equivalent to a fluence of 1 to $1.5 \times 10^7/cm^2$ 1 MeV neutron with

respect to displacement damage [4].

Previous studies of radiation damages of PIN photodiodes and APDs used either gamma rays or electrons (^{60}Co) or neutrons as the radiation source [5]-[13]. Based on those studies, it is estimated that the Si APDs for the GLAS laser altimeter will suffer a considerable increase in the bulk leakage current after 3 krad though the resultant degradation in the overall receiver performance is still tolerable. On the other hand, the damage to the Geiger mode APD single photon counter for the cloud lidar receiver is expected to become catastrophic after several hundred rad, because each electron of the bulk leakage current will be counted as a dark count. Other APD parameters such as the quantum efficiency, the gain, the device speed, and the breakdown voltage are not expected to change significantly for the relatively low dose that the GLAS receiver is subject to [8] [9].

There has been no direct measurement of proton radiation damage of Si APDs. It is of interest to compare the measurement results with the estimates based on the neutron radiation damage test. It is also of interest to test the proton-neutron equivalence relationship by Raymond for photodiodes, especially APDs which are normally operated at a much higher electrical field intensity than other types of semiconductor devices.

The rest of this report describe the test setup, the measurement procedure, the test results, and the estimated space radiation damage for the GLAS laser altimeter and cloud lidar receivers.

2 Experiment Setup

The proton radiation source used was the Tandem Van de Graaff accelerator at the Brookhaven National Laboratory [14]. The tests were conducted on April 25-26, 1994. Three proton energy levels were chosen: 14.8 MeV, 22 MeV, and 28 MeV. The flux was set to $10^6 - 10^7$ protons/$cm^2 sec$.

The test samples consisted of nine EG&G C30902STC devices, three for each proton energies. These devices are used by EG&G in their single photon counting module SPCM-100-PQ. Each device contained a C30902S Si APDs on a small thermal electric cooler, all in a TO type package. The diameter of the APD active area was 0.5 mm and the thickness of the active volume was 27 μm. The active volume was, therefore, $5.3 \times 10^{-6} cm^3$. The glass window in front of the APD was 1.0 mm thick and was made of Bora-Silicate glass, which had a density of 2.6 and a composition of O(60%), Si(26%), B(9%), Na(3%), and Al(1%). The window attenuated the proton energy to 5.1, 16.2, and 23.4 MeV, respectively [14]. The glass windows were not under the direct influence of the thermal electrical cooler.

Figure 1 shows the circuit layout of the test fixture. The circuit used was a typical passive quenching photon counting circuit given in the EG&G data sheet [15]. The APDs were tested at both 22°C and -10°C. Three APDs were mounted on the test fixture and were irradiated simultaneously. The proton beam had a radius of 17.5 cm and was uniform within 2% across the beam. The three APDs were on a 9.525 cm radius circle and were well within the beam. The photoelectron pulses were brought out via the 50Ω coax cable A1, B1, and C1. The other three coax cables, A2, B2, and C2, were used to carry the returns of the APD bias currents which were to be measured by the electrometer. This configuration helped to reduce the leakage current and settlement time in the low current measurements because there was no common mode voltage in the current measurement. As the current increased to above $1.0 \mu A$, the voltage drop across the $200 K\Omega$ resistor became significant and it should be subtracted from the voltage measured by the voltage meter.

Figure 2 shows the test instrument setup. A personal computer (PC) was used to automatically control the measurement and to log the test data. The bias voltage for the APD was generated by the Analog Module 521-5 programmable high voltage supply and was controlled by the D-to-A output of the PC. The resolution of the bias

voltage output was 0.10 volts. The bias voltage was monitored independently by the HP3478A digital multimeter. The Keithely 617 electrometer which measure the APD current was put in series in the return of the APD bias supply. The voltage burden of the electrometer was less than 1.5 mV. The photoelectron pulses were amplified and then fed to the SR620 universal counter. A 50 MHz lowpass filter was used to reduce the noise counts caused by the circuit thermal noise. The oscilloscope displayed in real time the photoelectron pulses and it also measured the pulse height distribution. In order to avoid ground loop, the chassis of all the instruments were isolated from the power line ground and tied together at one point to the vacuum chamber. The signal ground which was carried by the shield of the coax cable A1, B1, and C1 were also connected to vacuum chamber at the feed through plate. Only one APD could be tested at a time by connecting the appropriate type D and BNC connectors, as shown in Figure 2. During the irradiation, all three APDs were biased at about 120 volts simultaneously through the use of a special three way adapter cable (not shown).

The dark current increase versus dose for the APDs in linear mode could also be determined by biasing the APD below the breakdown point. The dark current consisted of the bulk leakage current and the surface leakage current. The former passed through the APD high field avalanche section and was the source of the dark counts for Geiger APDs. The latter did not pass through the avalanche region and might be assumed nearly unchanged as the bias voltage changed around the break-down point. As a worst case, one may approximate that all the radiation induced dark current was from the bulk leakage current. The net increase in the bulk dark current was equal to the difference of the measured dark currents before and after the irradiation divided by the average APD gain.

Each measurement consisted two parts: determining the device break-down voltage and then taking a set of measurements at a series of bias voltages around the break-down point. The first part of the measurement was carried out as follows.

(1). The device temperature was set (manually) to either $22°C$ (thermistor=$11.4K\Omega$) or $-10°C$ (thermistor=$50.9K\Omega$).

(2). The high voltage module output a voltage.

(3). The HP3478A DMM measured the bias voltage.

(4). The SR620 universal counter counted the number of pulses received. The counting interval was set to 0.1 seconds. The threshold level was set to 150 mV, which was relatively high but necessary to eliminated the noise counts due to the circuit thermal noise and RF pick-up from the environment.

The process continued by repeating Steps (2) through (4) at another setting of the high voltage. We began at roughly 10 volts below the break-down point, and incremented at 1 volt steps until the number of counts exceeded 3000/s. The break-down voltage was determined as the voltage at which the counting rate was 100/s. This point was obtained through linear interpolation between the two points below and above 100 counts/s. One could observe the pulses on the oscilloscope display once the bias voltage exceeded the break-down point. This definition of the break-down voltage might be slightly higher than the true value. Nevertheless, it served as a reference point in our measurements.

Once the breakdown point was determined, the second part of the measurement was proceeded as follows.

(1). The high voltage module output a voltage.

(2). The HP3478A DMM measured the bias voltage.

(3). The Keithely 617 electrometer measured the current through the APD. Ten measurements were taken and the mean and the standard deviation were calculated.

(4). The SR620 universal counter counted the number of pulses received. The gate time and the threshold were set to 0.1 seconds and 150 mV, respectively. Ten measurements were taken and the mean and the standard deviation were calculated.

(5). The oscilloscope (HP54720A) measured the mean and variance of the pulse

(5). The oscilloscope (HP54720A) measured the mean and variance of the pulse amplitude distribution.

Steps (1) through (5) were repeated for each bias voltage setting. The voltages selected were 50, 150, $V_b - 1$, $V_b - 0.5$, V_b, $V_b + 0.5$, $V_b + 1$, $V_b + 2$, $V_b + 3$, $V_b + 4$, $V_b + 5$, $V_b + 6$, volts with V_b the measured break-down voltage. Later in the experiment, we also added points at $V_b - 10$, $V_b - 5$, $V_b - 4$, $V_b - 3$, and $V_b - 2$ volts.

The performance of those APDs as single photon counter was tested prior to the irradiation using a He-Ne laser ($\lambda = 632$ nm). The photoelectron detection probability versus bias voltage was measured up to $V_b + 6$ at 22°C. The measurement results and the pulse shape were close to those given in the APD data sheet [15]. The pulse width measured at 10% points was about 1.0 μs. The residual noise current of the entire setup was about 0.40 nA when the laser was off and the bias voltage was zero.

3 Measurement Results and Discussions

We first measured the instantaneous dark count rate of three APDs at 14.8 MeV energy and at a flux of about 1000 $protons/s \cdot cm^2$. Such a flux corresponded to about 10^{-3} rad/s after the glass window and is the highest dose rate expected for the GLAS receiver as it orbits through the South Atlantic Anomaly [1]. There were no significant increase in the measured dark counts. This was expected since the number of protons which hit the APD active area were only $1.96 protons/s$. The dark count rate of the APD, on the other hand, was typically a few hundred to a thousand per second at −10°C. The radiation induced dark counts were not detectable under this condition unless one single proton could produce thousands of dark counts.

The proton flux was then increased to about $10^6/s$ and the measurement procedures described in the previous section were carried out with the proton beam blocked after a preset dose was accumulated. The first set of the three APDs were irradiated at 14.8 MeV and measured after 100, 200, 300, 400, 500, 1,000, 3,000, and 10,000

rad. The second set were irradiated at 22 MeV and measured after 50, 100, 200, 500, 1,000, 3,000, 10,000, and 30,000 rad. The third set were irradiated at 28 MeV and measured after 16, 31, 62, 155, 311, 933, and 3,110 rad. The measurements were repeated at 1 week and 1 month after the irradiation to determine the annealling effect. Lastly, the three APDs which were irradiated by the 22 MeV protons were measured one more time after being heated up in an oven at $100°C$ for 1 hour.

Figures 3 and 6 show the measured dark currents and dark counts of one of the APD (#4, at 22 MeV) as a function of the measured bias voltage at $22°C$ and $-10°C$, respectively. The other eight APDs showed similar characteristics. The decrease in the dark counts at 22°C as the dose increased from 3 krad 30 krad, as shown in Figure 4, was clearly caused by the circuit saturation when compared to Figure 6. As the dark counts exceeded certain level, the pulse amplitudes began to decrease because of a limited supply current. As a result, the number of pulses which crossed the discriminator threshold decreased as the actual dark counts increased. This also explained why the dark counts at 22°C increased from 1 week to 1 month after the irradiation. The slight decrease of the dark current below the break-down point at −10°C (Figure 5) was believed to result from the test circuit, not the APD, because the measured currents were too close to the residual noise current of the setup (0.4 nA).

One may concluded from those figures that: (a) Significant increases in the dark counts began as early as 50 rad; (b) The dark counts at $-10°C$ became excessively high, about half a million per second, after 3 krad; (c) There were little changes in the break-down voltages with the radiation doses; (d) The increase in the total dark currents below the break-down voltage was not significant until 3 krad; (e) There was some annealling, about 25% in the dark counts and about a factor of 2 in the dark current (below break-down point) for this particular device. Heating the device accelerated the annealling process.

The ratio of the dark counts at $-10°C$ and $22°C$ corresponded roughly to the relationship given in [16],

$$I_{bulk}(T) \propto e^{-0.55eV/kT} \tag{1}$$

where T is the absolute temperature in Kelvin and k is Boltzmann's constant. One may used this equation to predict the dark current and dark counts at other temperatures. As an example, the dark count rate increases by 13.7 from $-10°C$ to $22°C$.

Figure 7 shows plots of the dark counts vs. doses using the same data set as Figure 3. The number of the dark counts were corrected for the detector dead-time using the formula [17]

$$\hat{n} = \frac{n}{1 - n(\tau_d/T_o)} \tag{2}$$

where $\hat{n}$ is the maximum likelihood estimate of the dark counts, n is the actually measured dark counts, τ_d is the dead time, and T_o is the counting interval. The dead-time was taken to be $\tau_d = 1.0\mu s$, which was roughly the same as the pulse width of the Geiger mode APDs in this setup. Since the dead-time correction became increasingly inaccurate as the value of $n(\tau_d/T_o)$ approaches unity, we eliminated in Figure 7 those data points with $n > 0.5 \times 10^6/s$. Furthermore, due to the slight variation in the break-down voltage at different doses, the dark counts were not all measured at exactly the same set of the voltage points. As a result, the voltage point set used in the zero dose measurement were used as the reference and the data points for the nonzero doses were obtained using the interpolation function of the KaleidaGraph software package [18]. It is shown in Figure 7 that the dark counts increased almost linearly with the doses and the bias voltage only affected the detection probability.

The net increase in the dark count rate vs. proton dose may be obtained by first subtracting the count rate at zero rad and then dividing it by the corresponding photoelectron detection probability. The photoelectron detection probabilities were measured prior to the irradiation using a He-Ne laser and it was 18.9% for this APD

at $22°C$ and at 5 volts above the break-down point. The measured photoelectron detection probabilities for lower bias voltages were not used since they were less accurate and depended increasingly on the threshold setting and the accuracy of the break-down voltage measurement. According to [15], the detection probability was a function of the voltage above the break-down point and independent of the temperature. We further assumed that the photoelectron detection probability was unchanged before and after the irradiation. Figure 8 plots the net dark count rate increase vs. dose up to 3 krad. The straight line which passes the origin was obtained by a least square fit. The proton radiation damage coefficient which was the slope of the line was $1.76 \times 10^3 counts/s \cdot rad$.

Table 1 shows the net dark count increase vs. dose for all the nine Si APDs. The 22 MeV protons caused more damage than the other two energies. The total detected APD dark counts at a different temperature and a different bias voltage may be estimated by multiplying the results in Table 1 by

$$P_d(V - V_b) \cdot exp[-\frac{0.55eV}{k}(\frac{1}{T(°K)} - \frac{1}{263.5})] \tag{3}$$

where $P_d(V - V_b)$ is the photoelectron detection probability. For other models of Si APDs. the proton radiation damage may be calculated by scaling the above result for the appropriate active volume.

We also measured the detected photon counts due to the fluorescence of the glass window by putting an irradiated APD face-to-face against a undamaged APD on the test fixture. The fluorescence photon counts were no more than 200/s measured immediately after 10 krad 14.8 MeV proton irradiation. Therefore, the effect of fluorescence from the glass window was negligible.

It would required much higher proton doses to determine the bulk leakage current increase vs. dose for the APDs in linear mode when the biased voltage was about 10 volts below the break-down point (APD gain$\approx$ 100). As shown in Figures 5 and 6, the increase in the dark current only became apparent at voltages very close to the

Table 1: Test Result of the APD dark counts increase due to proton irradiation

Proton Energy *before Window* *after Window*	14.8 MeV 5.1 MeV			22 MeV 16.2 MeV			28 MeV 23.4 MeV		
APD Serial #	#1	#2	#3	#4	#5	#6	#7	#8	#9
$\Delta cts/s \cdot rad$	1540	1230	1500	1760	2530	1600	761	871	885
Average	1420			1960 (1630†)			839		

†Exclude APD#5.

break-down point for the proton radiation doses we used. The average APD gain at such a high bias voltage was too high to maintain a stable linear operation. However, one may assume the bulk leakage current was unchanged as the bias voltage decreased to below the break-down point. The bulk leakage current due to the irradiation can be obtained by multiplying the net APD dark count rate by the electron charge, e.g. 0.26 fA/rad at $-10°C$ and 22 MeV. The corresponding dark current at room temperature ($22°C$) should be 3.6 fA/rad according to Eq.(1).

The noise current spectral density due to the irradiation is given by [19]

$$N_{rad} = 2qG^2F\Delta I_{bulk} \quad (A^2/Hz) \tag{4}$$

where q is the electron charge, G is the average APD gain, and F is the APD excess noise factor given by $F = k_{eff}G + (2 - 1/G)(1 - k_{eff})$ with k_{eff} the APD ionization coefficient ratio. The corresponding noise equivalent power (NEP) is equal to $\sqrt{N_{rad}}$ divided by the APD responsivity, i.e.,

$$NEP_{rad} = \frac{\sqrt{N_{rad}}}{qG(\eta/hf)} = \frac{\sqrt{2qG^2F\Delta I_{bulk}}}{qG(\eta/hf)} \quad (Watts/\sqrt{Hz}) \tag{5}$$

where η is the APD quantum efficiency and hf is the photon energy.

The measurement data were several times smaller than that calculated according to the neutron test results and the proton-neutron equivalence relationship by Raymond. Kraner [12] showed that, for neutrons, $\Delta I_{bulk} = \alpha\Phi V$ with α a leakage current constant, Φ the neutron fluence, and V the device volume. Buchinger and et al. [13]

showed that $\alpha = 1.7 \times 10^{-16}\ A/cm$ for this kind of APDs at room temperature. Raymond [4] showed that 1 rad protons over 1-100 MeV range had about the same effect in displacement damage as $1.5 \times 10^{7}/cm^{2}$ neutron fluence. Therefore, the predicted APD bulk current due to the proton irradiation is 13.5 fA/rad at room temperature, which is about 4 times of what we measured (3.6 fA/rad).

On the other hand, the radiation damage we measured was much higher than those obtained with gamma rays. The APD used in the Mars Observer Laser Altimeter (MOLA) was claimed to have no performance degradation after 100 krad total dose according to the specification from the McDonnell Douglas Astronautics Company. Conner and Guggenmos [20] also reported that, for a Si APD very similar to those we tested, the total dark current increased by only about 30% after 100 krad at room temperature. There was no further details given about those tests.

4 Estimated Space Radiation Damage of Si APDs for GLAS

4.1 The GLAS Cloud Lidar Receiver

One of the candidate photodetector for the GLAS lidar receiver is a single photon counting module which contains a newly developed large area ($\phi = 0.5mm$) EG&G $Slik^{TM}$ Si APD with an active quenching circuit [21]. The thickness of the device active region is $25\mu m$ and the active volume is $4.9 \times 10^{-6}\ cm^{3}$, The active quenching circuit enables the photon counter to have a short dead-time, about 30 ns, which corresponds to a useful maximum count rate of $15 \times 10^{6}/s$. The bias voltage is assumed to be 15 volts above the break-down point, which gives a photoelectron detection probability of 80% and a photon detection probability of 68% at $\lambda = 532nm$. For low dark count rates, the APD is mounted on a two stage cooler and the temperature is held at $-40°C$.

We assume that the proton irradiation has the same effect for the *Slik* APD.

Because of the smaller active volume and lower temperature, the dark counts of this $Slik^{TM}$ photon counter due to proton radiation is predicted to be 0.175 times those listed in Table 1. For example, at 14.8 MeV, the detected dark count is estimated to be about $250/s \cdot rad$. The dark counts of the single photon counting module will be about 750,000/s after 3 krad at the end of the GLAS mission, which is about 3 orders of magnitude higher than the dark count rate before launch. This would seriously affect the overall receiver performance, especially during nighttime measurement when the detected noise photons from moon lit clouds is only $\sim 1000/s$. Although the radiation induced dark counts are still less than the detected signal photons and daytime background noise photons, the effect of radiation damage has to be considered when designing the receiver. Further increase of the shielding thickness is not effective for high energy protons [1]. Further decrease of the device temperature can reduce the dark counts, for example, by a factor of 56 from $-40°$C to $-70°$C, but the detector subsystem may become too complicated. On the other hand, if one uses a single stage thermal electric cooler and the APD temperature is held at $-20°C$, the dark counts would be $2160/s \cdot rad$, or $6.5 \times 10^6/s$ after 3 krad. At room temperature, the single photon counting module will start to saturate ($15 \times 10^6/s$) after as little as 200 rad.

The transient increase in the dark count when GLAS passes the South Atlantic Anomaly can be neglected according to the real time measurement described at the beginning of the previous section. The Si APD photon counting modules are definitely suitable for short space missions.

4.2 The GLAS Altimeter Receiver

The Si APD to be used in the GLAS altimeter receiver is the same as that used in MOLA. Its basic structure is similar to those we tested but the active volume is thicker, 140 μm. Typical quantum efficiencies of 35% at $\lambda = 1.064nm$ is assumed, though 43% has been reported as the highest [22]. The ionization coefficient ratio is

roughly $k_{eff} = 0.007$. The diameter of the active area is $\phi = 0.8mm$. The active volume is therefore $7 \times 10^{-5} cm^3$. The APD is operated in linear mode at room or slightly higher temperature for high quantum efficiency at $1.064\mu m$ wavelength. The bias voltage is set for an average gain of $G \approx 200$. The receiver electrical bandwidth is about 150 MHz. The expected increase in the APD bulk leakage current according to our test result is 0.041 pA/rad for 14.8 MeV protons at $22°C$.

If we assume the space radiation damage by the protons over the entire energy spectrum is, on the average, the same as that at 14.8 MeV, the total bulk leakage current due to space radiation will be 120 pA after 3 krad. The rms noise due to this increase in I_{bulk} according to Eq.(4) will be $2.3pA/Hz^{1/2}$, which is almost the same as the total equivalent input noise current density of the APD preamplifier module ($2.6pA/Hz^{1/2}$) prior to irradiation. The corresponding NEP caused by the radiation damage is 38 $fW/Hz^{1/2}$, or 0.47 nW over the 150 MHz bandwidth. The received background noise power from clouds is estimated to be about 3 nW at daytime and 3 pW at nighttime. Therefore, the GLAS altimeter receiver will show some radiation related degradation, but much less severe than that of the single photon counting module for the cloud lidar receiver.

References

[1] J. L. Barth and E. G. Stassinopoulos, *Space Radiation Exposure of the GLAS Mission*, X-900-93-06, NASA-Goddard Space Flight Center, Radiation Physics Office, Earth Science Directorate, Aug. 1993.

[2] E. G. Stassinopoulos and J. P. Raymond, 'The space radiation environment of electronics,' *Proceedings of the IEEE*, Vol. 76, No. 11, pp. 1423-1442, Nov. 1988.

[3] G. C. Messenger and S. A. Ach, *The Effects of Radiation on Electronic Systems*, 2nd ed., Van Nostrand Reinhold, New York, 1992.

[4] J. P. Raymond and E. L. Petersen, 'Comparison of neutron, proton, and gamma ray effects in semiconductor devices,' *IEEE Trans. Nuclear Science*, Vol. NS-34, No. 6, pp. 1622-1628, Dec. 1987.

[5] A. H. Kalma, and W. H. Hardwick, 'Radiation testing of PIN photodiodes,' *IEEE Trans. Nuclear Science*, Vol. NS-25, No. 6, pp. 1483-1488, Dec. 1978.

[6] C. E. Barnes, 'Radiation Effects in 1.06-μm InGaAs LED's and Si photodiodes,' *J. Appl. Phys.*, Vol. 50, No. 8, pp. 5242-5250, Aug. 1979.

[7] C. E. Barnes, 'Radiation effects on light sources and detectors,' in *Radiation Effects in Optical Materials*, P. W. Levy, ed., SPIE Vol. 138, pp. 138-149, 1985.

[8] L. W. Aukerman, Y. Song, F. L. Vernon, Jr., G. A. Evans, and J. Z. Wilcox, 'Radiation effects on semiconductor optical devices for space communications,' in *Laser and Laser Systems Reliability*, SPIE Vol. 328, pp. 56-65, 1982.

[9] L. W. Aukerman, F. L. Vernon, Jr., and Y. Song, 'Radiation threshold levels for noise degradation of photodiodes,' *Optical Engineering*, Vol. 23, No. 5, pp. 678-684, Oct. 1984.

[10] J. J. Wiczer, 'Radiation-hardened optoelectronic components: detectors,' in *Optical Technologies for Communication Satellite Applications*, SPIE Vol. 616, pp. 254-266, Jan. 1986.

[11] E. A. Swanson, E. R. Arnau, and F. G. Walther, 'Measurements of natural radiation effects in a low noise avalanche photodiode,' *IEEE Trans. Nuclear Science*, Vol. NS-34, No. 6, pp. 1658-1661, Dec. 1987.

[12] H. W. Kraner and Z. Li, 'Fast neutron damage in silicon detectors,' *Nuclear Instruments and Methods in Physics Research*, Vol. A279, pp. 266-271, 1989.

[13] F. Buchinger, H. Dautet, J. K. P. Lee, R. J. McIntyre, and M. Orchard-Webb, 'Real-time monitoring of single-neutron-induced damage in silicon using avalanche photodiodes operating in the Geiger mode,' *Nuclear Instruments and Methods in Physics Research*, Vol. B72, pp. 496-498, 1992.

[14] *SEU Test Facility: User Guide*. SEU Test Facility, Brookhaven National Laboratory, New York, Dec. 1, 1992.

[15] EG&G C30902S, C30921S data sheet, EG&G Canada Ltd., Vaudreuil, Quebec, Canada, March 1988.

[16] A. Lightstone, A. MacGregor, D. MacSween, R. McIntyre, C. Trottier, and P. Webb, 'Photon counting modules using RCA silicon avalanche photodiodes,' *Electronic Engineering*, Vol. 61, pp. 37-47, Oct. 1989.

[17] D. L. Snyder, *Random Point Process*, John Wiley & Sons, New York, 1975, p. 252.

[18] *KaleidaGraph Reference Guide*. 3rd ed., Synergy Software, Reading, PA, 1993.

[19] P. P. Webb, R. J. McIntyre, and J. Conradi, 'Properties of avalanche photodiodes,' *RCA Review*, Vol. 35, pp. 234-278, June 1974.

[20] J. L. Conner and J. L. Guggenmos, 'Direct detection avalanche photodiode receiver design for the NASA/DDLT,' in *Optomechanical Design of Laser Transmitters and Receivers*, SPIE Vol. 1044, pp. 145-154, 1989.

[21] H. Dautet, P. Deschamps, B. Dion, A. D. MacGregor, D. MacSween, R. J. McIntyre, C. Trottier, and P. P. Webb, 'Photon counting techniques with silicon avalanche photodiodes,' *Applied Optics*, Vol. 32, No. 21, pp. 3894-3900, July 20, 1993.

[22] S. D. Hammond, 'Improved avalanche photodiode and hybrid preamplifier for 1064 nm wavelength,' in *Free-space Laser Communication Technologies, II*, SPIE Vol. 1218, pp. 635-643, 1990.

Circuit Diagram of the Test Fixture (Rev 3, 4/5/94)
(Bottom View)

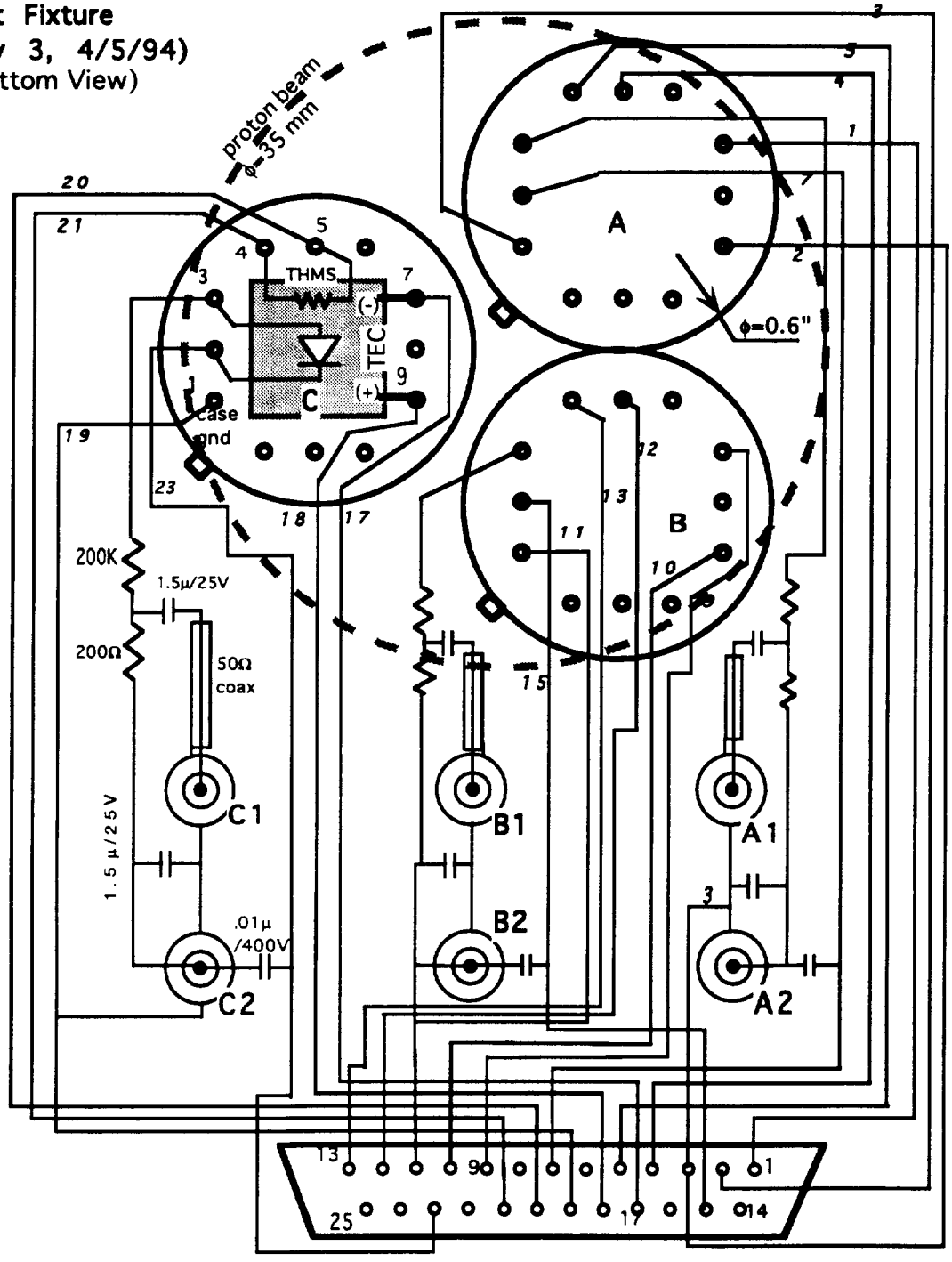

Figure 1. Circuit Layout of the Test Fixture.

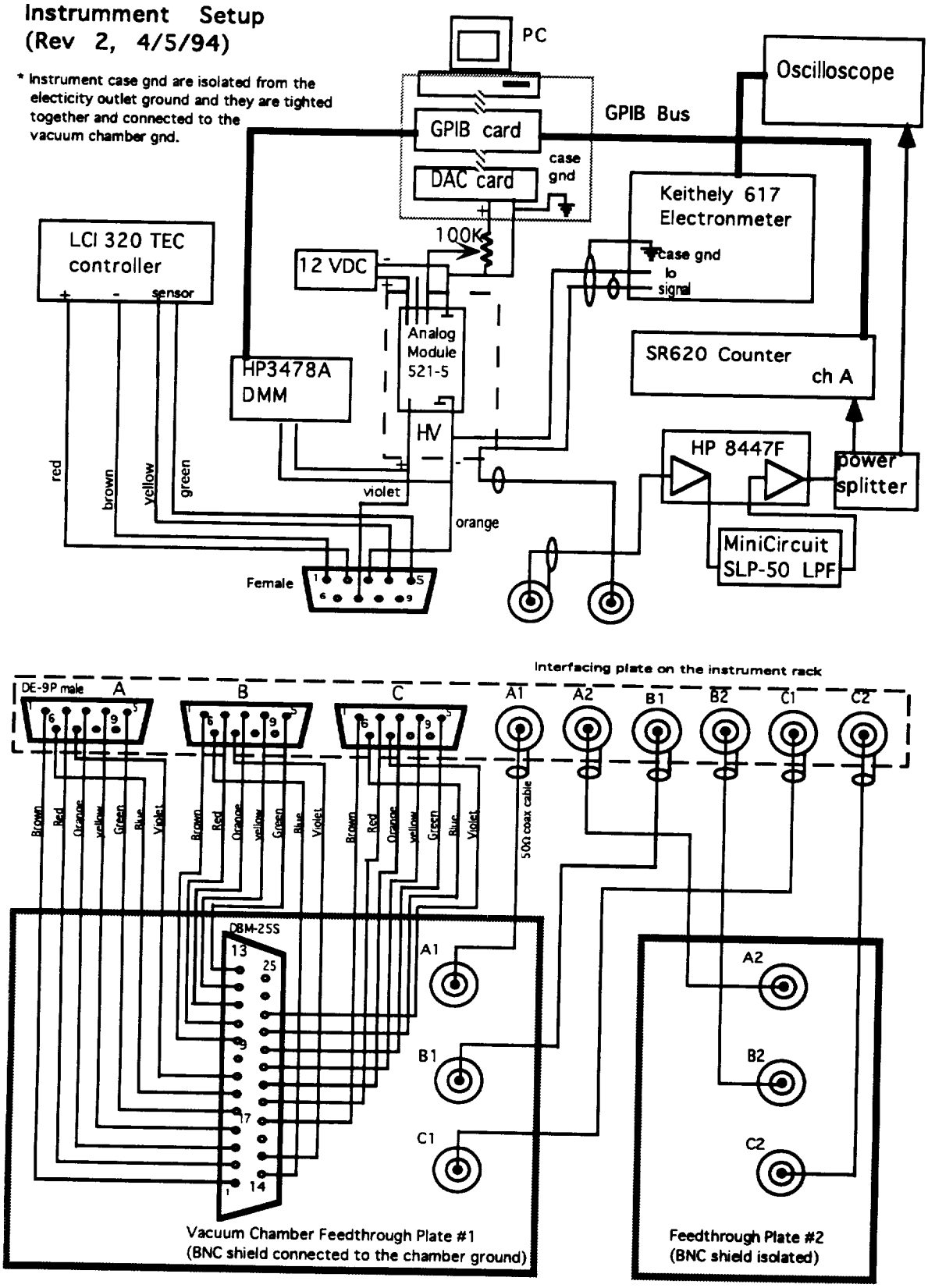

Figure 2. Test Instrument Setup and Cable Connections.

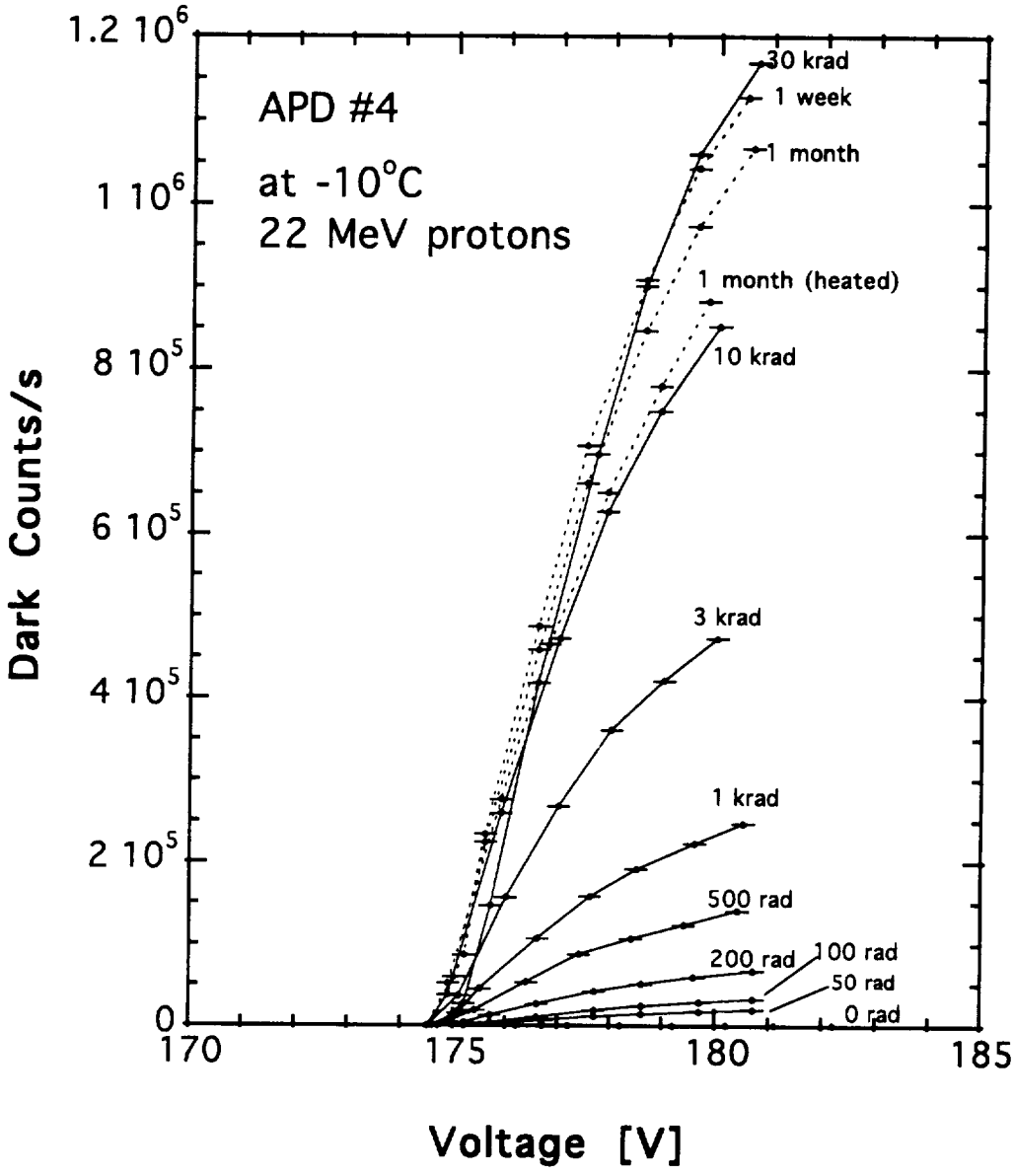

Figure 3. Dark counts vs. voltage of APD #4 at -10° C.

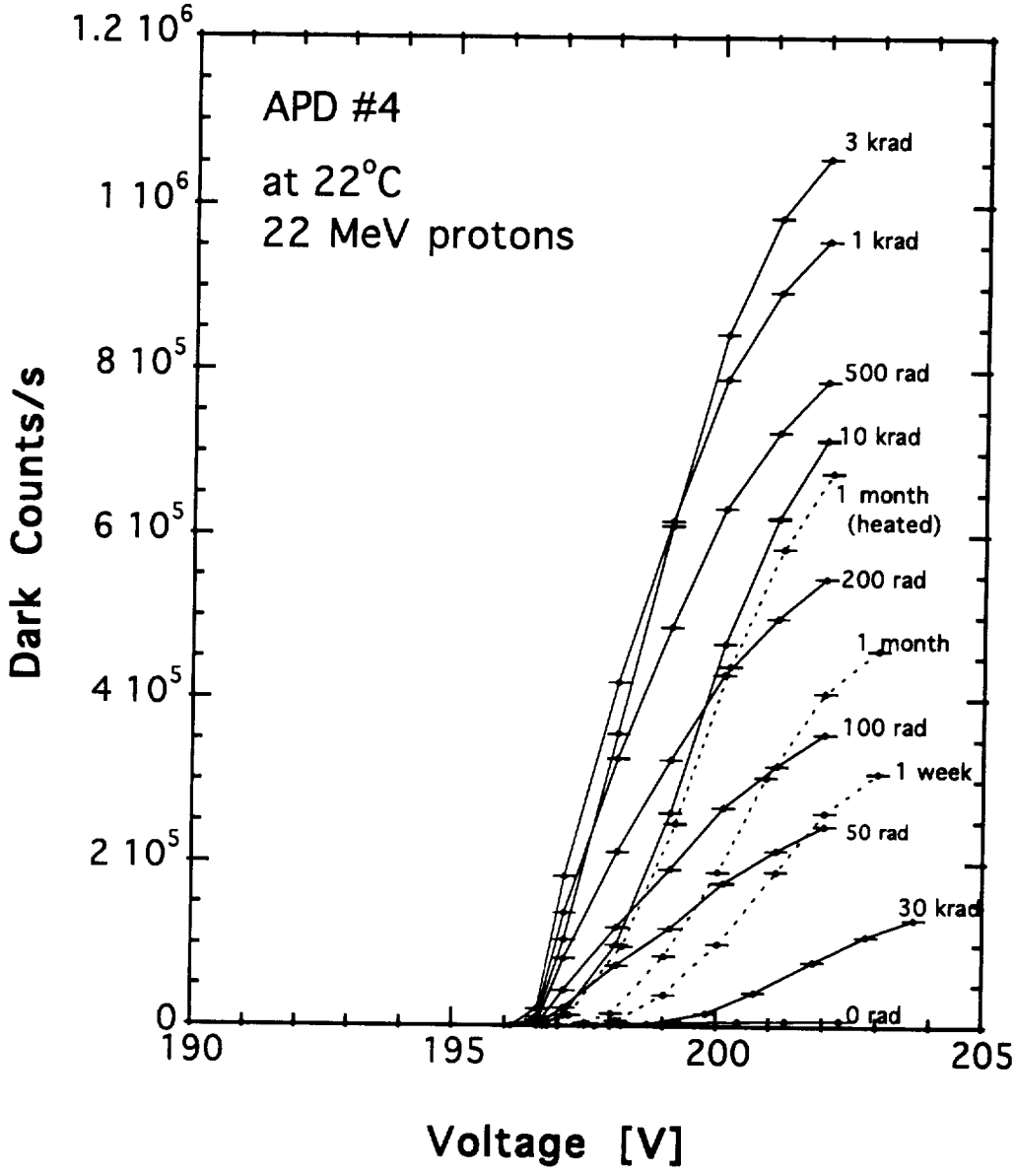

Figure 4. Dark counts vs. voltage of APD #4 at 22° C.

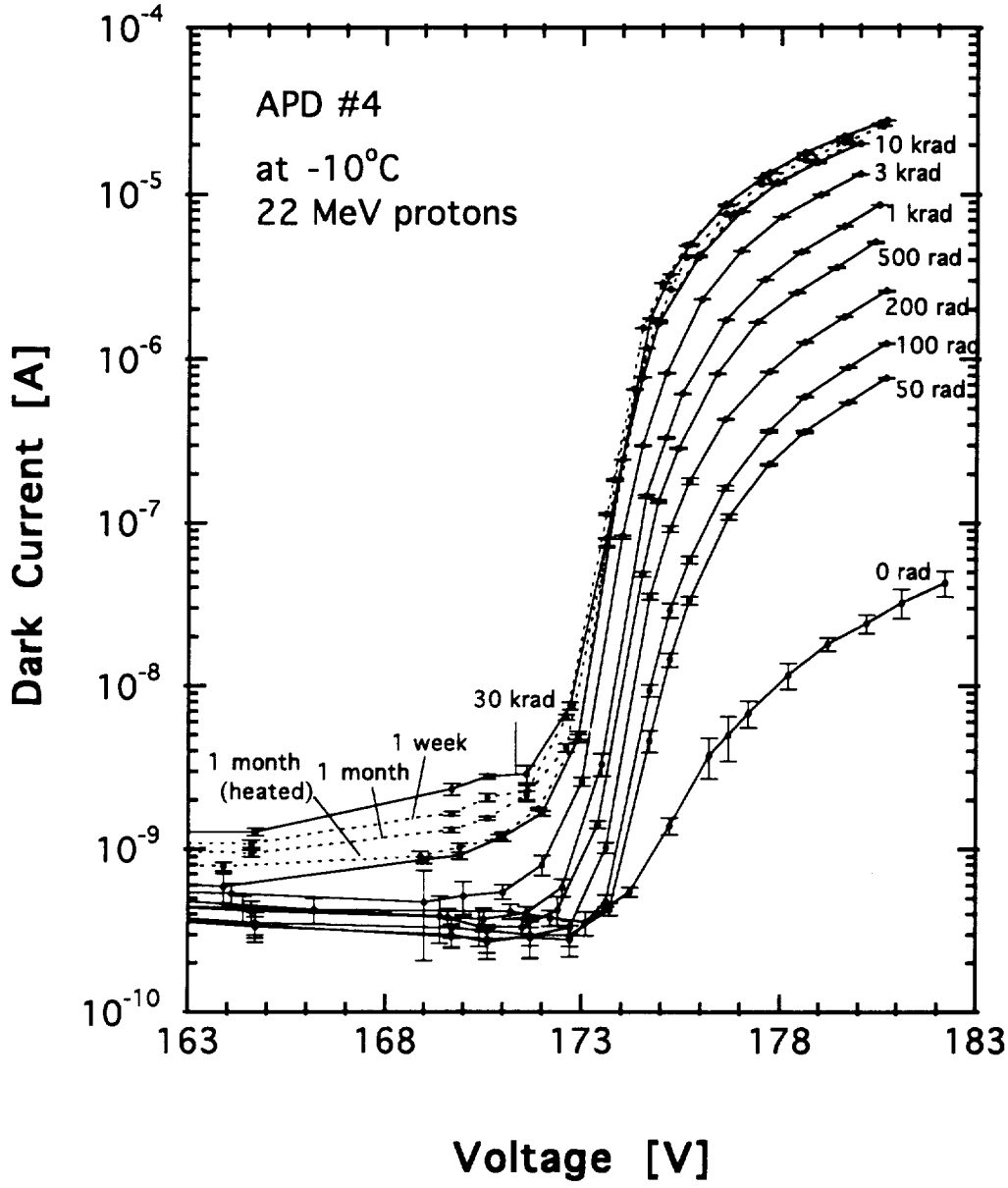

Figure 5. Dark current vs voltage of APD #4 at -10°C.

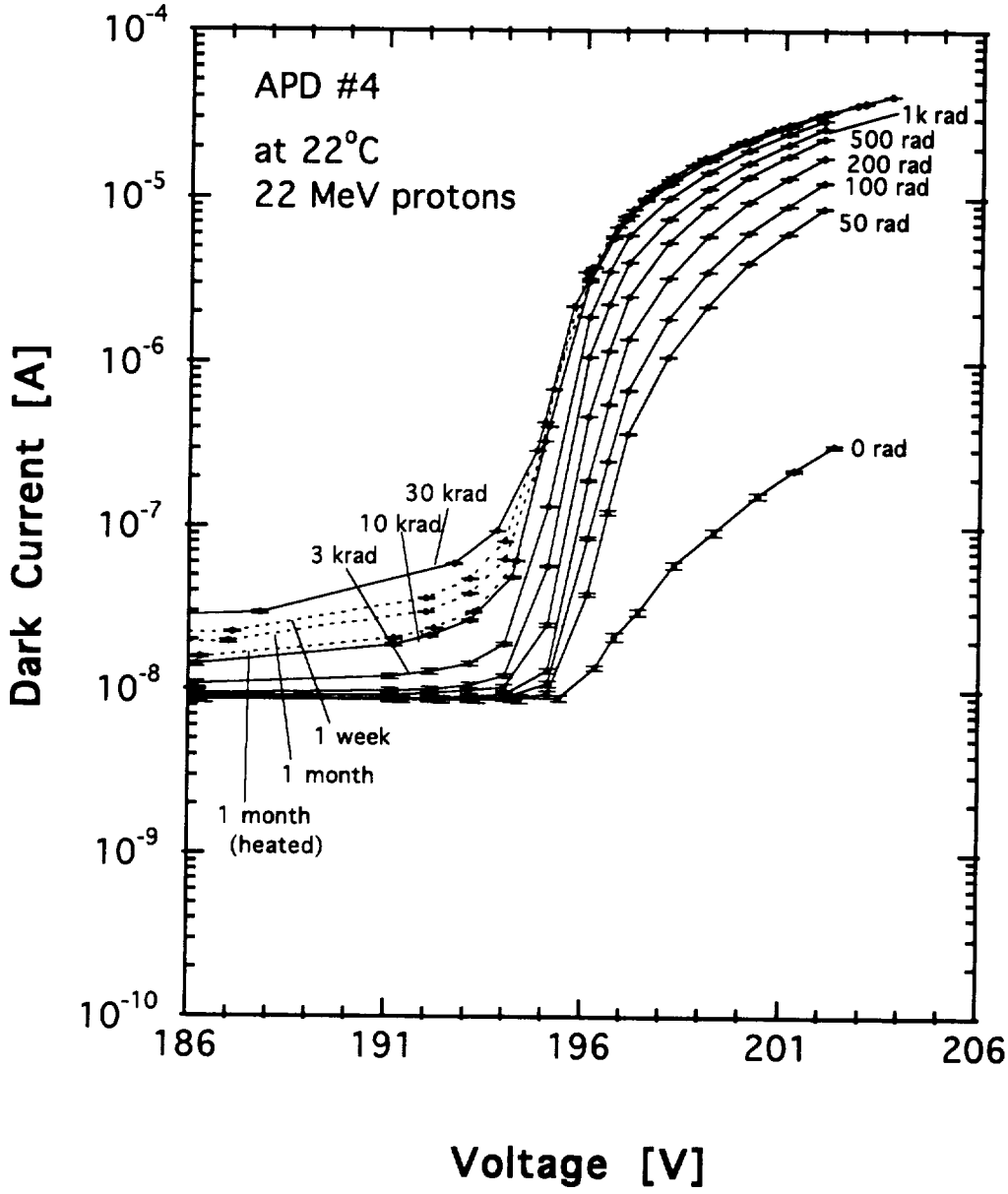

Figure 6. Dark current vs voltage of APD #4 at 22°C.

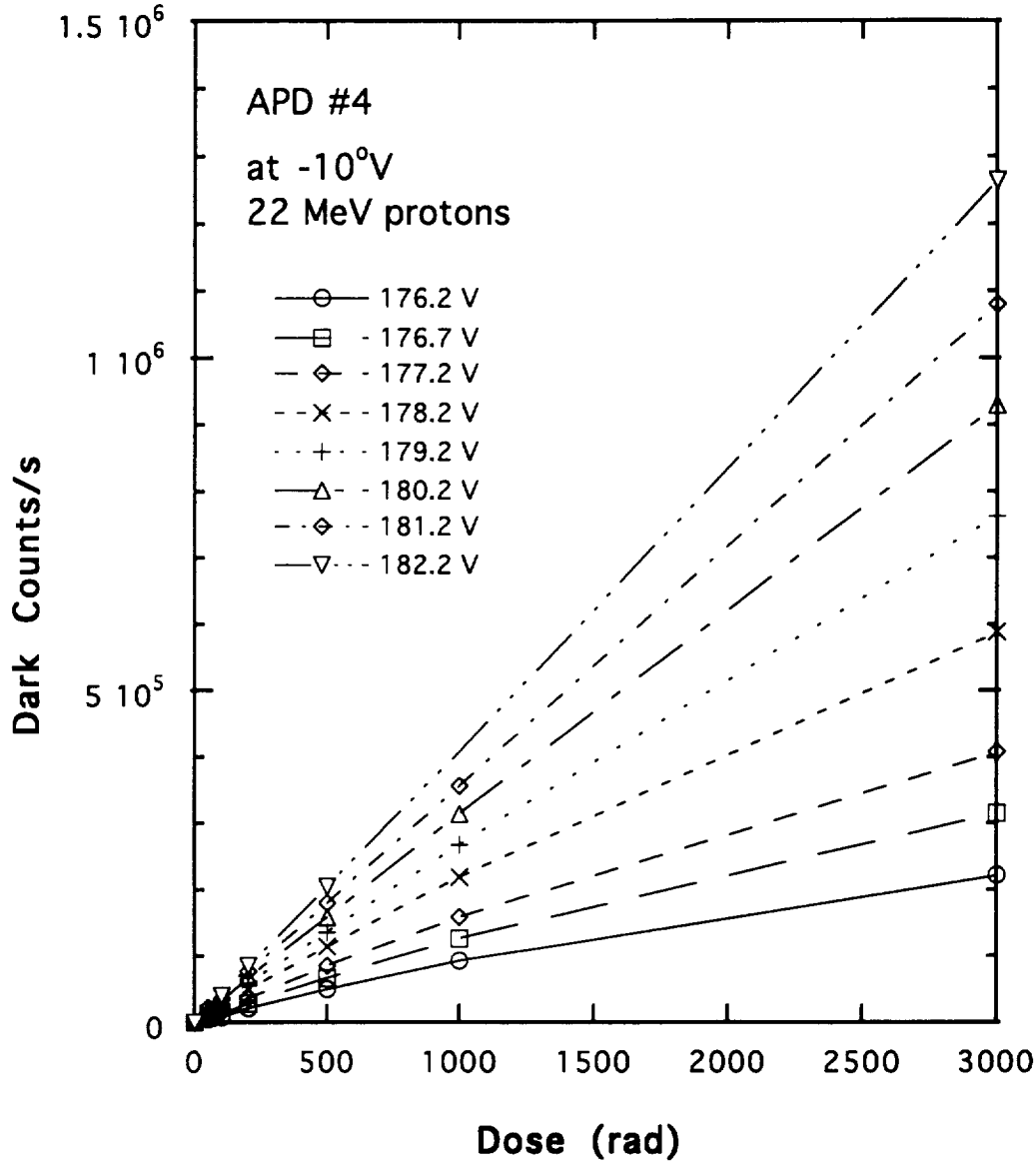

Figure 7. Dark counts vs. dose of APD #4 at -10°C.

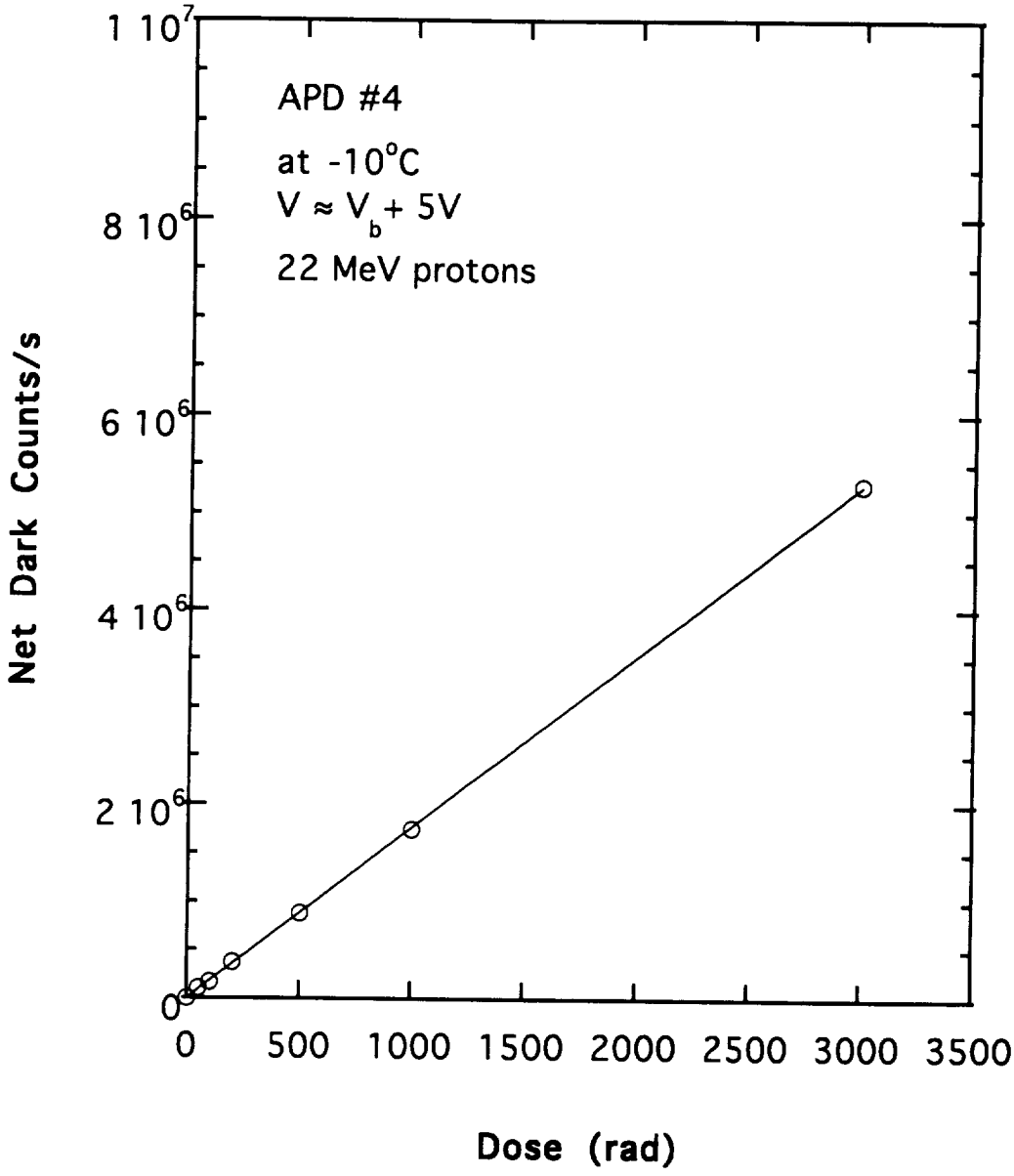

Figure 8. Net dark counts vs. dose. The net dark counts is defined as the measured dark counts divided by the photoelectron detection probability, which was measured to be P_d=18.9% at V ≈ V_b+5 V.

Computer Simulation of Avalanche Photodiode and Preamplifier Output for Laser Altimeters

Xiaoli Sun
Dept. ECE, The Johns Hopkins University
Revision 1, October 1994

1. Introduction

The following is a description of the computer program which simulate the output signal from an avalanche photodiode (APD) and preamplifier in a laser altimeter receiver. The signal consists of random number of photoelectrons output from the APD and the noise from the preamplifier. The former follows the McIntyre-Webb distribution [1][2][3] and the latter follows the Gaussian distribution. The two can be assumed independent of each other. The output of the simulation program consists of an array of discrete samples at a given sampling rate. Each sample is equal to the signal averaged over the sampling interval. In the calculation, we define the signal as the input current to the preamplifier. All the noise sources will be converted to equivalent current noises at the input to the preamplifier.

Figure 1 shows a block diagram of the program. The input signal is an array of discrete sample of the received optical power. Each sample represents the average value of the actual signal over the sampling interval. The program consists of a McIntyre-Webb random number generator for the APD secondary photoelectrons and a Gaussian random number generator for the preamplifier noise. A

digital lowpass filter is also included to simulate the noise filter in the laser altimeter receiver.

2. Simulation of the Preamplifier Noise

The preamplifier noise follows the Gaussian distribution. Press and et al. [4] have shown a subroutine for generating standard Gaussian random variable. We need only to scale this standard Gaussian random variable, y_{g0}, to obtain the preamplifier noise output, y_g, according to the relationship

$$y_g = \sigma y_{g0} + \mu \tag{1}$$

where μ and σ are the mean and standard deviation of the preamplifier noise. The mean of amplifier noise can be considered to be zero. The variance has to be calculated in frequency domain because only the preamplifier noise spectral density is given.

Since each sample represents the average signal over the sampling interval, i.e.

$$x_i = \frac{1}{\Delta\tau}\int_{t_i}^{t_i+\Delta\tau} x(t)dt \tag{2}$$

the sampled preamplifier noise should also be the average amount of noise over the sampling interval. This is equivalent to have a filter after the preamplifier with rectangular impulse response of duration $\Delta\tau$ and amplitude $1/\Delta\tau$. The Fourier transform of this filter is given by

$$H_s(\omega) = \frac{\sin(\omega\Delta\tau/2)}{\omega\Delta\tau/2} \tag{3}$$

It is the analog to digital sampling process that results in this filter. The bandwidth of the filter is roughly $1/\Delta\tau$, which should be much wider than the actual receiver electrical bandwidth.

The variance of the sampled preamplifier Gaussian noise can be calculated as

$$\sigma^2 = \frac{1}{2\pi}\int_0^{\infty} |H_s(\omega)|^2 N(\omega) d\omega \qquad (A^2) \qquad (4)$$

where $N(\omega)$ is the one sided noise power spectrum of the preamplifier.

If the preamplifier contains a FET as the front stage, the noise power spectrum can be written as [5]

$$N(\omega) = \frac{4KT_a}{R_f} + 2qI_g + \frac{4KT_a\Gamma}{g_m R_f} + \frac{4KT_a\Gamma}{g_m}(\omega C_i)^2 \qquad (A^2/Hz) \qquad (5)$$

where K is the Botzmann's constant, T_a(°K) is the ambient temperature, R_f is the transimpedance of the preamplifier, g_m is the transconductance of the FET, Γ is a factor close to unity, and C_i is the total capacitance at the input of the preamplifier.

When the altimeter receiver bandwidth is below 200 MHz, one can often approximate the preamplifier noise as white Gaussian noise with the variance given as

$$\sigma^2 = \frac{4KT_n}{R_f}\frac{1}{2\Delta\tau} \qquad (A^2) \qquad (6)$$

where T_n(°K) is the equivalent noise temperature. We used Eq. (6) to calculate the rms preamplifier noise in the program.

3. Simulation of the Photocurrent Output from the APD

The sampled output of an APD is a discrete random process which is equal to the numbers of secondary photoelectrons output by the APD during the sampling interval times the electron charge and then divided by the sampling interval. The probability of the number of photoelectrons has been shown to follow the so-called McIntyre distribution [1][2], as

$$P(m|\lambda(t)\Delta\tau) = \sum_{n=1}^{m} P_M(m|n) \cdot \frac{(\lambda(t)\Delta\tau)^n}{n!} e^{-\lambda(t)\Delta\tau}, \qquad m \geq 1$$

$$P(0|\lambda(t)\Delta\tau) = e^{-\lambda(t)\Delta\tau} \tag{7}$$

with $P_M(m|n)$ the probability of generating m secondary photoelectrons in response to n primary photoelectrons, given by

$$P_M(m|n) = \frac{n\Gamma\left(\frac{m}{1-k_{eff}}+1\right)}{m(m-n)!\,\Gamma\left(\frac{k_{eff}m}{1-k_{eff}}+1+n\right)} \cdot \left[\frac{1+k_{eff}(G-1)}{G}\right]^{n+\frac{k_{eff}m}{1-k_{eff}}} \cdot \left[\frac{(1-k_{eff})(G-1)}{G}\right]^{m-n} \tag{8}$$

where k_{eff} is the APD hole to electron ionization coefficient ratio, G is the average APD gain, and $\lambda(t)$ is the primary photon counting rate given by

$$\lambda(t) = \frac{\eta}{hf}\left[P_s(t) + P_0\right] + \frac{I_b}{q} \tag{9}$$

where η is the APD quantum efficiency, hf is the photon energy, $P_s(t)$ is the input optical signal power, P_0 is the background radiation

power assuming to be constant, I_b is the APD bulk leakage current, and q is the electron charge.

A very close approximation to (7) was given by Webb and et al. [3] for $\lambda(t)\Delta\tau>>1$, as

$$P_w(m|\lambda(t)\Delta\tau) \approx \frac{1}{\sqrt{2\pi G^2 F\lambda(t)\Delta\tau}} \cdot \frac{1}{\left[1+\frac{(m-G\lambda(t)\Delta\tau)(F-1)}{GF\lambda(t)\Delta\tau}\right]^{\frac{3}{2}}}$$
$$\cdot \exp\left[-\frac{(m-G\lambda(t)\Delta\tau)^2}{2G^2F\lambda(t)\Delta\tau\left[1+\frac{(m-G\lambda(t)\Delta\tau)(F-1)}{GF\lambda(t)\Delta\tau}\right]}\right], \quad m>\lambda(t)\Delta\tau \tag{10}$$

where F is the APD excess noise factor which can be calculated as

$$F = k_{eff}G + \left(2-\frac{1}{G}\right)(1-k_{eff}). \tag{11}$$

It is also known [6] that the Webb's approximation becomes inaccurate as $\lambda(t)\Delta\tau$ <<1. Therefore, we choose to use Eq. (10) only for $\lambda(t)\Delta\tau$ >10.

Because the complexity of the probability distributions for the APD, one cannot generate the random variable as an analytical function of a uniform distributed random variable. Instead, the rejection method described in [4] has to be used. A comparison function has to be found when using this method. A comparison function is an upper bound for the desired probability distribution function and the total area under the curve has to be finite. The inverse function of the indefinite integral of the comparison function should also be known analytically. The area (integral) of the comparison function should

be as small as possible since the time required to generate a random number is proportional to the area.

We simulate the APD photoelectron output for $\lambda(t)\Delta\tau \leq 10$ in two steps. First we generate a Poisson variables to simulate the number of primary photo electrons. We then generate a McIntyre random number for each primary photoelectron according to (8). The APD output should be the sum of secondary photoelectrons in respond to all primary photoelectrons. This procedure involves calling a Poisson random number generator once and then calling a McIntyre random number generator n times with n the outcome of the Poisson random number generator. This method only requires a comparison function for the McIntyre distribution for the n=1 case.

The Poisson random number generator can be implemented using the computer subroutine provided by Press and et al. [4]. The McIntyre random number generator can be realized similarly but with the McIntyre probability distribution function and an appropriate comparison function. We may still use a Lorentzian distribution as the comparison function as in [4], i.e.,

$$f(x) = \frac{c_0}{1 + \frac{(x - x_0)^2}{a_0^2}} \tag{12}$$

but we need to find a set of values for c_0, x_0, and a_0 such that $f(m) > P_M(m|1)$ and $\int_{-\infty}^{\infty} f(x)dx$ is as small as possible. As an example, we found $c_0=4/G$, $x_0=-G/50$, and $a_0=G/3$ may be used for APD gains from G=50 to 500.

The expression for McIntyre distribution (8) has to be rewritten or it will easily cause overflow in the computer as m become large. Using the property of the Gamma function, one can rewrite P(m|n=1), Eq. (8), as

$$P(m|1)=\frac{\Gamma\left(\frac{k_{eff}m}{1-k_{eff}}+m+1\right)}{m!\,\Gamma\left(\frac{k_{eff}m}{1-k_{eff}}+2\right)}\left[\frac{1+k_{eff}(G-1)}{G}\right]^{1+\frac{k_{eff}m}{1-k_{eff}}}\left[\frac{(1-k_{eff})(G-1)}{G}\right]^{m-1}$$

$$=\frac{\left(\frac{k_{eff}m}{1-k_{eff}}+m\right)\left(\frac{k_{eff}m}{1-k_{eff}}+(m-1)\right)\cdots\left(\frac{k_{eff}m}{1-k_{eff}}+2\right)\Gamma\left(\frac{k_{eff}m}{1-k_{eff}}+2\right)}{m!\,\Gamma\left(\frac{k_{eff}m}{1-k_{eff}}+2\right)}$$

$$\cdot\left[\frac{1+k_{eff}(G-1)}{G}\right]^{1+\frac{k_{eff}m}{1-k_{eff}}}\left[\frac{(1-k_{eff})(G-1)}{G}\right]^{m-1}$$

$$=\frac{\left(\frac{m}{1-k_{eff}}\right)\left(\frac{m}{1-k_{eff}}-1\right)\cdots\left(\frac{m}{1-k_{eff}}-(m-2)\right)}{m(m-1)\cdots(m-(m-2))}$$

$$\cdot\left[\frac{1+k_{eff}(G-1)}{G}\right]^{1+\frac{k_{eff}m}{1-k_{eff}}}\left[\frac{(1-k_{eff})(G-1)}{G}\right]^{m-1}$$

$$=\prod_{l=0}^{m-2}\frac{\left(\frac{m}{1-k_{eff}}-l\right)}{(m-l)}\cdot\left[\frac{1+k_{eff}(G-1)}{G}\right]^{1+\frac{k_{eff}m}{1-k_{eff}}}\left[\frac{(1-k_{eff})(G-1)}{G}\right]^{m-1}$$

$$=\prod_{l=0}^{m-2}\left(1+\frac{k_{eff}l}{m-l}\right)\cdot\left[\frac{1+k_{eff}(G-1)}{G}\right]^{1+\frac{k_{eff}m}{1-k_{eff}}}\left[\frac{(1-k_{eff})(G-1)}{G}\right]^{m-1} \quad (13)$$

For $\lambda(t)\Delta\tau > 10$, one may simulate the APD output in one step using the Webb's approximation, Eq. (10), to save computation times. The comparison function is again chosen to be Lorentzian, Eq. (12), but with $c_0=1/G(F\lambda(t)\Delta\tau)^{1/2}$, $x_0=G\lambda(t)\Delta\tau$, and $a_0=G(2F\lambda(t)\Delta\tau)^{1/2}$, which is adequate for average APD gains from 10 to 500 and average primary photoelectrons from 10 to 100, or a even wider range (yet to be tested).

APDs also have surface leakage current which is not multiplied by the APD gain. This part of the APD dark current should be modeled as a DC current which results in an additive Gaussian noise of mean and variance

$$\mu = qI_s\Delta\tau$$
$$\sigma_s^2 = qI_s\Delta\tau \qquad (14)$$

where I_s is the surface leakage current.

4. Simulation of the Lowpass Noise Filter

The lowpass noise filter is simulated using the impulse invariance method [7], i.e., the impulse response of the discrete time filter being equal to the samples of the impulse response of the corresponding continuous time filter, as

$$h(n) = \Delta\tau h_c(n\Delta\tau) \qquad (15)$$

where $h_c(t)$ is the impulse response of the continuous time filter to be simulated. This method gives the closest simulation of the actual filter in the receiver as long as both the signal and the filter are band limited and the sample rate is sufficiently high.

Usually, a buildable lowpass filter are specified by the locations of the poles and zeros each of which results from a physical capacitor or inductor. One can derive the system function and obtain the filter impulse response by taking the inverse Fourier transform of the filter system function. The discrete time filter impulse response can then be obtained according to Eq. (15). The impulse response function of a bandwidth limited filter is ideally infinite in time. However, we may truncate it as the values becomes vanishingly small and turn it into a finite impulse response (FIR) digital filter. The filter impulse response is derived separately and stored as an array.

The lowpass filter output is the convolution of the input signal with the impulse response function, as

$$y(n) = \sum_{k=n-N_h+1,\ k\geq 1}^{n} x(k)h(n-k+1) \qquad (16)$$

where x(n) and h(n) are the samples of the input signal and the impulse response of the filter. Here we assumed h(n)=0 if n<1 and n>N_h. The first N_h points in y(n) should be discarded because the input sequence is truncated, i.e. x(k)=0 if k<1.

The choice of the filter for a given input pulse shape and noise characteristics may be optimized by trail and error using this simulation program. Usually, a Gaussian or a Bessel lowpass filter is used for minimum pulse shape distortion. The former is easy to simulate but can only be implemented approximately. The latter can

be easily synthesized in practice and yet gives very close to Gaussian impulse response [8].

As an example, we implemented a fifth order Bessel lowpass filter. The poles of a normalized filter (ω_{3dB}= 1 rad/s) are located at $s_{1,2}$ = -0.9576766 ±j1.4711244, $s_{3,4}$ =-1.3808774 ±j0.7179096, and s_5 = -1.5023160 [9]. The normalized filter system function can be written as

$$H_0(s) = \frac{a_0}{(s-s_1)(s-s_2)\cdots(s-s_5)} = \frac{A_1}{s-s_1} + \frac{A_2}{s-s_2} \cdots \frac{A_5}{s-s_5} \tag{17}$$

The system function of the actual filter can be obtained by the frequency transformation $H(s)=H_0(s/\omega_c)$ with ω_c the 3 dB cutoff frequency. The impulse response is obtained by taking the inverse Laplace transform of H(s), as

$$h_c(t) = A_1\omega_c e^{s_1\omega_c t} + A_2\omega_c e^{s_2\omega_c t} + \cdots + A_5\omega_c e^{s_5\omega_c t} \tag{18}$$

The values of A_i's can be obtained through partial fraction, as $A_{1,2}$ = 0.6193736 ±j1.0986409, $A_{3,4}$ =-4.9168825 ±j(-2.6131445), and A_5= 8.5950178.

5. The Computer Program

Figure 2 shows a flowchart of the program. It is written in Fortran 77. The Poisson and Gaussian random number generators are from [4]. The uniform random variable generator is also from [4]. Other subroutines are developed by ourselves.

Figures 3 shows sample histograms of the Gaussian, the Poisson, the McIntyre, and the Webb random variable generators. They all agreed

very well with the corresponding theoretical distributions. The fluctuations at the tails of the histograms were due to the finite sample sizes.

Figure 4 shows the impulses of two low pass filters, a fifth order Bessel lowpass filter with 3 dB bandwidth equal to 100 MHz and an ideal integrator with integration time equal to 10 ns. Figures 5 and 6 show plots of the sample output from this APD preamplifier simulator using the lowpass filter given in Figure 4. The input optical signal had a rectangular pulse shape of width 10 ns. The received background radiation power was 1.0 nW and the peak signal power including the background was 20 nW. The pulse energy was therefore 1067 photons, or 373 primary photoelectron per pulse assuming 35% quantum efficiency. Other parameter values used are listed in Table 1.

References

[1] R. J. McIntyre, "The distribution of gains in uniformly multiplying avalanche photodiodes: Theory," *IEEE Trans. Electron Devices*, vol. ED-19, pp. 703-713, Sept. 1972.

[2] J. Conradi "The distribution of gains in uniformly multiplying avalanche photodiodes: Experimental," *IEEE Trans. Electron Devices*, vol. ED-19, pp. 713-718, Sept. 1972.

[3] P. P. Webb, R. J. McIntyre, and J. Conradi, "Properties of avalanche photodiodes," *RCA Review*, vol. 35, pp. 235-278, June 1974.

[4] W. H. Press, Saul A. Teukolsky, W. T. Vetterling, and B. P. Flannery, *Numerical Recipes in Fortran, The art of Scientific Computing*, 2nd ed., Cambridge University Press, New York, ch. 7 and ch. 12, 1992.

[5] R. G. Smith and S. D. Personick, "Receiver design for optical fiber communication systems," in , Spring-Verlag, New York, 1980, ch. 4.

[6] F. M. Davidson and X. Sun, "Gaussian approximation versus nearly exact performance analysis of optical communication systems with PPM signaling and APD receivers," *IEEE Trans. Commun.*, vol. COM-36, no. 11, pp. 1185-1192, Nov. 1988.

[7] A. V. Oppenheim and R. W. Schafer, *Discrete-Time Signal Processing*, Prentice-Hall, Englecliffs, NJ, 1989, ch. 7.

[8] H. J. Blinchikoff and A. I. Zverev, *Filtering in the Time and Frequency Domains*, John Wiley & Sons, New York, 1978, ch. 3.

[9] D. V. S. Humpherys, *The Analysis, Design, and Synthesis of Electrical Filters*, Prentice-Hall, Englewood Cliffs, NJ, 1970, p. 421.

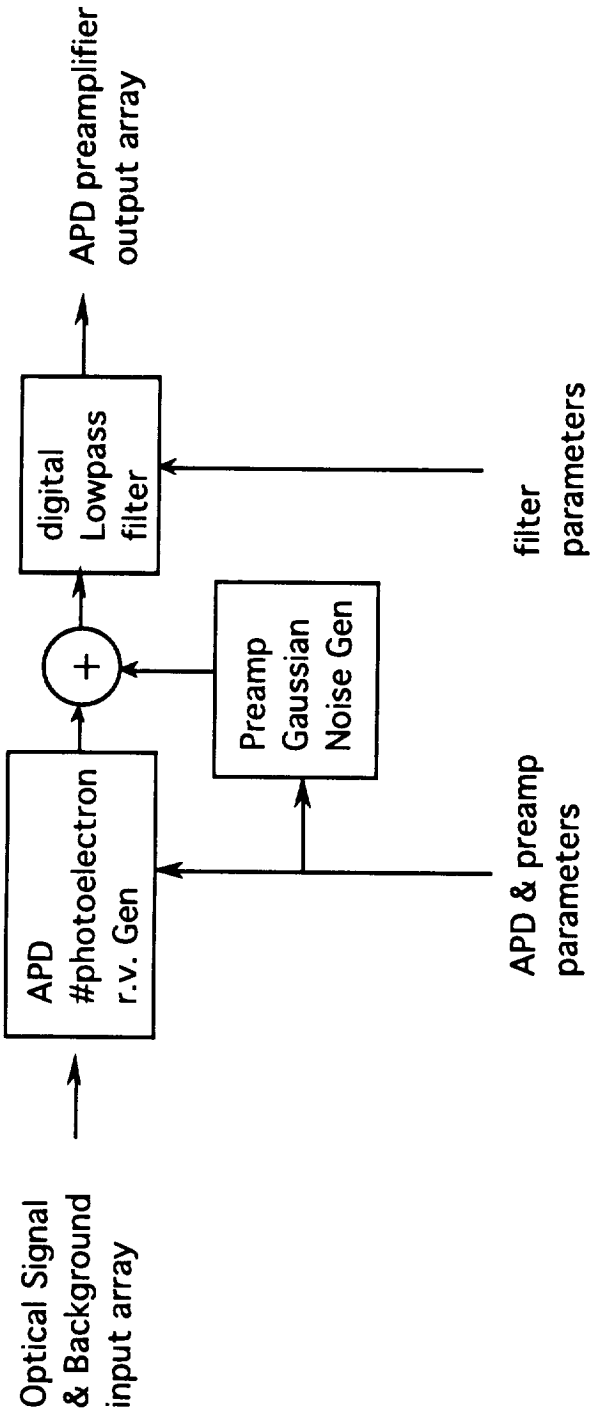

Figure 1. Block diagram of the APD preamplifier simulator

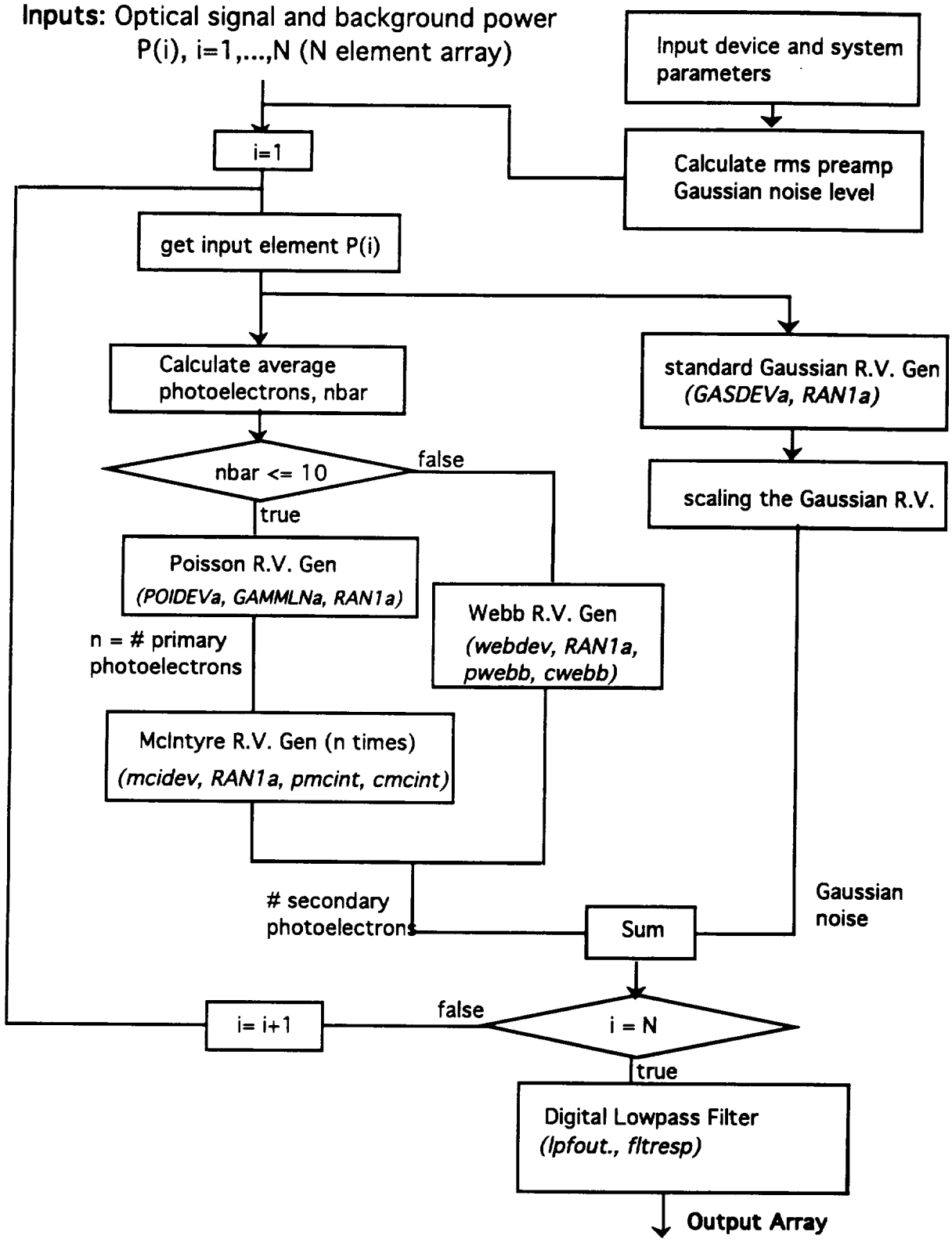

Figure 2. Block diagram of the APD preamplifier simulator program. The names of the subroutines and sub-subroutines are given in parenthesis.

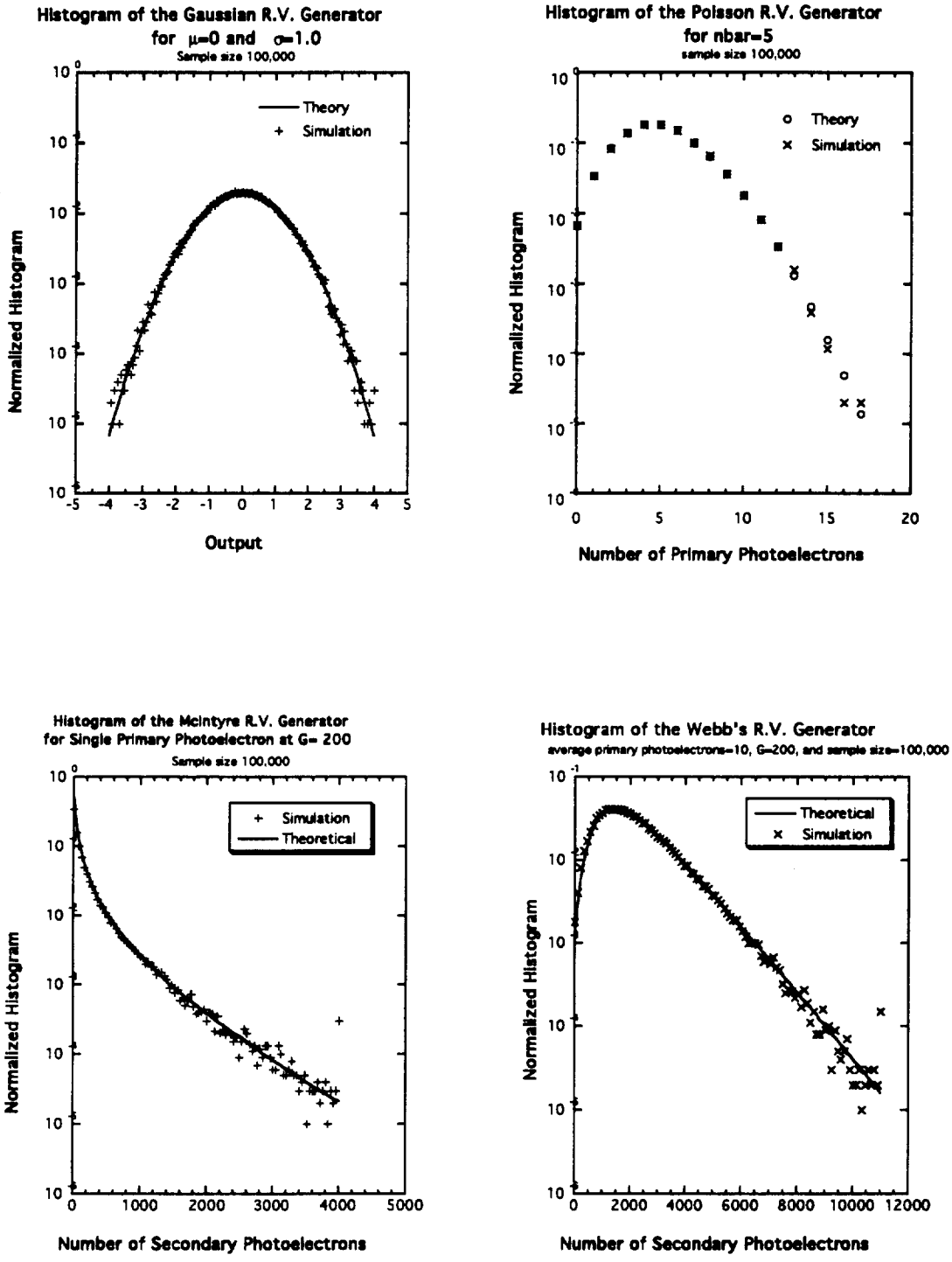

Figure 3. Sample histograms of the r.v. generators.

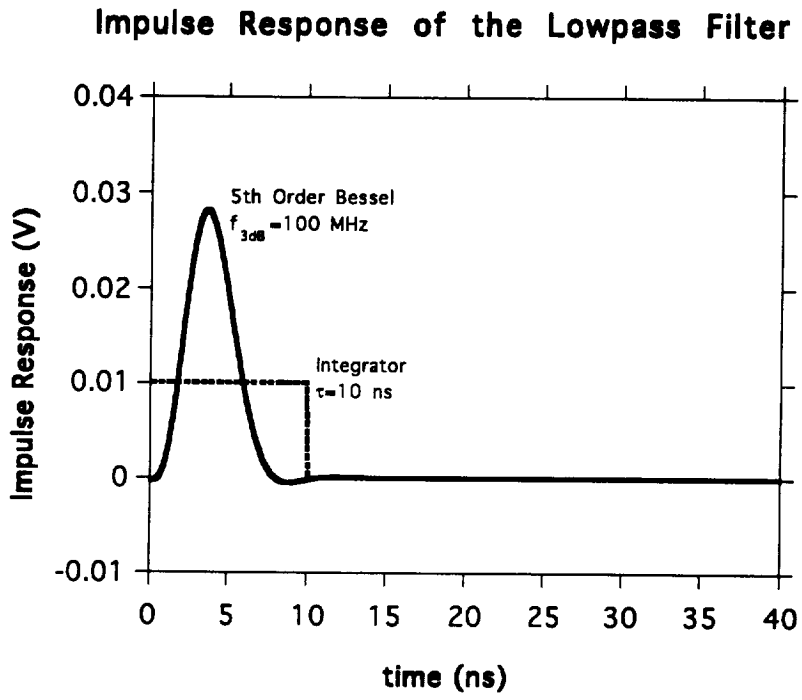

Figure 4. Impulse responses of a fifth order Bessel lowpass filter and an ideal integrator of integration time $\Delta\tau$=10 ns.

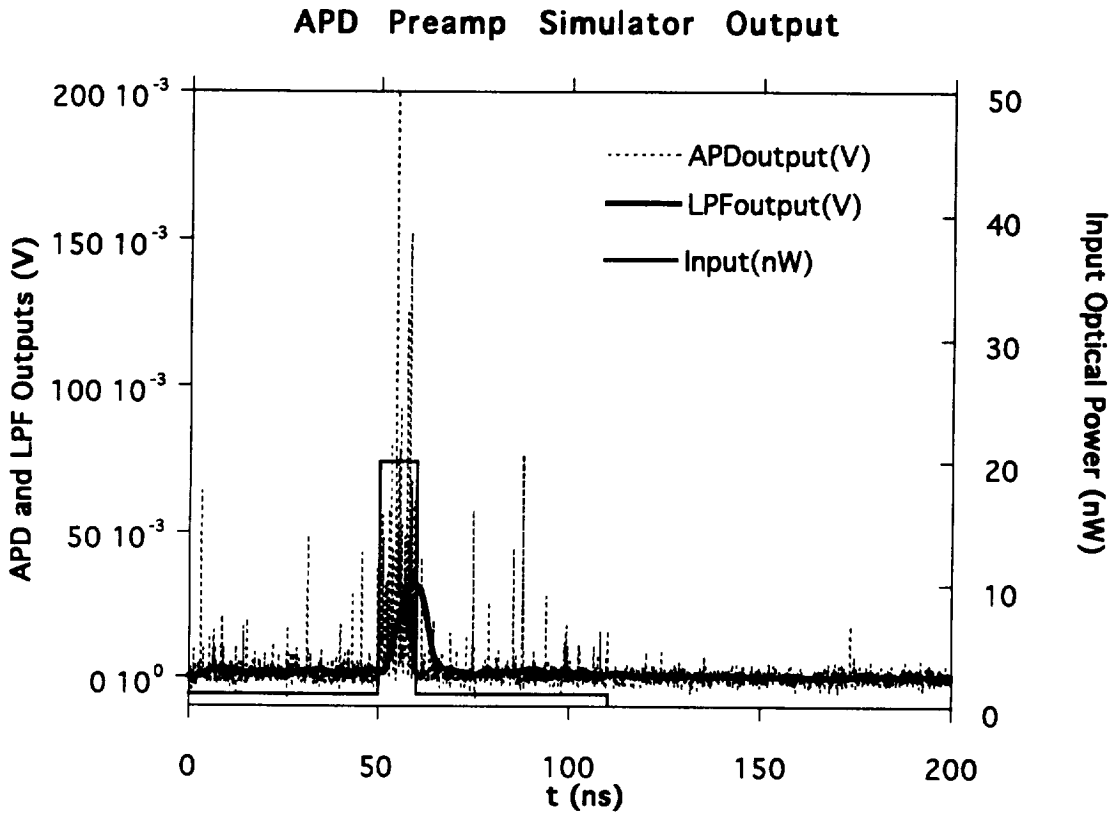

Figure 5. Sample APD preamp and lowpass filter outputs. The filter used was a fifth order Bessel lowpass filter with f_{3dB}=100 MHz.

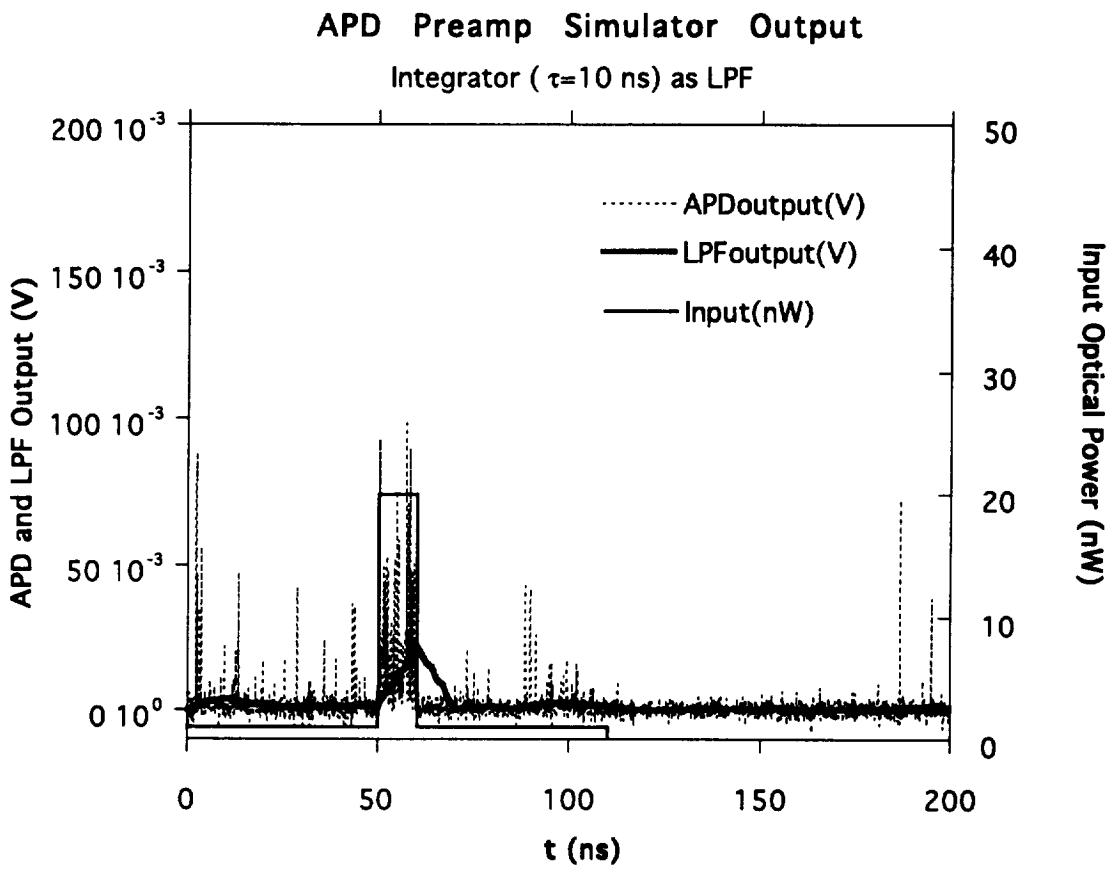

Figure 6. Sample APD preamp and lowpass filter outputs. The filter used was an ideal integrator with integration time $\Delta\tau$=10 ns.

Table 1. System Parameter Values for Figure 4.

laser pulse shape	rectangular
laser pulsewidth	10 ns
laser pulse peak power	19 nW
background radiation power	1.0 nW
wavelength, lambda	1060 nm
APD quantum efficiency, eta	35%
average APD gain, G	200
APD ionization coefficient ratio, k_{eff}	0.010
APD surface leakage current, Is	15 nA
APD bulk leakage current, Ib	50 pA
preamplifier feedback resistor, R	20 kohm
preamplifier noise temperature, Tn	700 ^{o} K
noise filter type	5th order Bessel LPF
noise filter 3dB bandwidth, fc	100 MHz
# points sampled, N	2048
sampling interval, dt	0.10 ns

```
apdout:         apdout.o POIDEVa.o GAMMLNa.o RAN1a.o mcidev.o webdev.o GASDEVa.o \
                fltresp.o lpfout.o
        f77 -o apdout apdout.o POIDEVa.o GAMMLNa.o RAN1a.o mcidev.o webdev.o \
            GASDEVa.o fltresp.o lpfout.o
POIDEVa.o:      POIDEVa.f
        f77 -c POIDEVa.f
GAMMLNa.o:      GAMMLNa.f
        f77 -c GAMMLNa.f
RAN1a.o:        RAN1a.f
        f77 -c RAN1a.f
mcidev.o:       mcidev.f
        f77 -c mcidev.f
webdev.o:       webdev.f
        f77 -c webdev.f
GASDEVa.o:      webdev.f
        f77 -c GASDEVa.f
fltresp.o:      fltresp.f
        f77 -c fltresp.f
lpfout.o:       lpfout.f
        f77 -c lpfout.f
```

October 21, 1994 apdout.f
X. Sun

```
**********************************************************************
*  This program generate an array of random variable to simulate     *
*  the APD and the preamp output equivalent at the input to the      *
*  preamp (in ampere) in response to an input array of samples of    *
*  incident optical power in watts                                   *
**********************************************************************
c
      INTEGER N, I, idum, m, I1, n1, kk, NLPF
      PARAMETER  (N=40000,NLPF=1000)
      REAL lambda, eta, G, Keff, Is, Ib, R, Tn, q
      PARAMETER  (q=1.6e-19)
      REAL dt, nbar
      REAL hf, F, sigma, mu, x1
      REAL PS(N), Y(N), Y1(N), RESPNS(NLPF)
c
c Received optical signal and background radiation power
c
      DATA  PS  /  500*1.0e-9,100*2.0e-8,500*1.0e-9,8900*0.0,30000*3.3e-9  /
c
      REAL mcidev, poideva, gasdeva, webdev  !subroutines to be called
c
c System Parameters and definitions of some of the variables used
c
c lambda=laser diode wavelength (nm)
c eta=APD quantum efficiency
c G=average APD gain
c Keff=ratio of ionization coefficients of APD
c Is=APD surface leakage current in nanoamperes (A)
c Ib=APD bulk leakage current in nanoamperes (A)
c R= Preamp transimpedance (APD load resistance) (Ohm)
c Tn=equivalent noise temperature (Kalvin)
c q=electron charge (C)
c dt=sampling interval (s)
c nbar=average # of primary photoelectrons in dt
c PS(I)=input optical signal array
c N=number of elements in PS(I)
c
      lambda=1060.0
      eta=0.35
      G=200
      Keff=0.010
      Is=15.0e-9
      Ib=0.050e-9
      R=20000.0
      Tn=700.0
      dt=0.10e-9
c
      print *, 'Seed for the random number generator?'
      read *, idum
c
c  Other parameters used in the calculation
c
      hf=1242.0/lambda*q     ! photon energy
      F=Keff*G+(2.0-1.0/G)*(1.0-Keff)   ! APD excess noise factor
```

```
        sigma=sqrt(2.0*1.38e-23*Tn/R/dt+q*Is/dt) ! rms Gaussian noise
      mu=Is                    ! mean of the Gaussian noise
c
c Start calculation
c
      do 500 I=1,N
c
c  Number of secondary photoelectrons from the APD
c
      nbar=eta*PS(I)/hf*dt+Ib*dt/q
      m=0
      if( nbar.LE.10.0 ) then
            n1= poideva(nbar,idum)
            if(n1.EQ.0) go to 200
            do 100 I1=1,n1
100         m=m+mcidev(G,Keff,idum)
      else
            m=webdev(nbar,G,F,idum)
      end if
c
c Preamp Gaussian noise
c
200   x1=sigma*gasdeva(idum)+mu
c
c  Total output voltage (volts)
c
      Y(I)=x1+real(m)*q/dt     ! current at the input to the preamp
      Y(I)=Y(I)*R              ! output voltage from preamp
500   continue
c
c The digital lowpass filter
c
      fc=100.0e6                    ! the 3dB cutoff frequency (Hz)
      call fltresp(NLPF, fc, dt, RESPNS)  ! Lowpass filter impulse response
      call lpfout(Y, N, RESPNS, NLPF, Y1)  ! convolution
c
c Print the Results
c
      write(20,700)
700   format(1x,'index',7x,'t(ns)',7x,'Input(nW)',5x,
     +          'APDoutput(V)',2x,'LPFoutput(V)' )
      do 900 kk=1,N
      write(20,800)  kk,  dt*kk*1.0e9,  PS(kk)*1.0e9,  Y(kk),  Y1(kk)
800   format(1x,  I6,  2f14.3,  2e14.3 )
900   continue
c
      stop
      end
```

X. Sun

```
      FUNCTION poideva(xm,idum)
      INTEGER idum
      REAL poideva,xm,PI
        PARAMETER (PI=3.141592654)
c
        REAL alxm,em,g,oldm,sq,t,y,gammlna,ran1a
      SAVE alxm,g,oldm,sq
       DATA oldm /-1./
        if (xm.lt.12.)then
         if (xm.ne.oldm) then
          oldm=xm
            g=exp(-xm)
        endif
         em=-1
         t=1.
2        em=em+1.
           t=t*ran1a(idum)
         if (t.gt.g) goto 2
      else
         if (xm.ne.oldm) then
         oldm=xm
            sq=sqrt(2.*xm)
           alxm=log(xm)
             g=xm*alxm-gammlna(xm+1.)
        endif
1           y=tan(PI*ran1a(idum))
         em=sq*y+xm
         if (em.lt.0.) goto 1
         em=int(em)
               t=0.9*(1.+y**2)*exp(em*alxm-gammlna(em+1.)-g)
          if (ran1a(idum).gt.t) goto 1
       endif
      poideva=em
       return
      END
```

X. Sun

```
      FUNCTION gammlna(xx)
      REAL gammlna,xx
      INTEGER j
       DOUBLE PRECISION ser,stp,tmp,x,y,cof(6)
      SAVE cof,stp
            DATA  cof,stp/76.18009172947146d0,-86.50532032941677d0,
             *24.01409824083091d0,-1.231739572450155d0,.120865097386617 9d-2,
             *-.5395239384953d-5,2.5066282746310005d0/
       x=xx
       y=x
        tmp=x+5.5d0
            tmp=(x+0.5d0)*log(tmp)-tmp
           ser=1.000000000190015d0
       do 11 j=1,6
         y=y+1.d0
           ser=ser+cof(j)/y
11     continue
         gammlna=tmp+log(stp*ser/x)
       return
      END
```

```
      FUNCTION ran1a(idum)
      INTEGER idum,IA,IM,IQ,IR,NTAB,NDIV
      REAL ran1a,AM,EPS,RNMX
           PARAMETER  (IA=16807,IM=2147483647,AM=1./IM,IQ=127773,IR=2836,
     *NTAB=32,NDIV=1+(IM-1)/NTAB,EPS=1.2e-7,RNMX=1.-EPS)
       INTEGER j,k,iv(NTAB),iy
      SAVE iv,iy
        DATA iv /NTAB*0/, iy /0/
        if (idum.le.0.or.iy.eq.0) then
          idum=max(-idum,1)
         do 11 j=NTAB+8,1,-1
         k=idum/IQ
             idum=IA*(idum-k*IQ)-IR*k
           if (idum.lt.0) idum=idum+IM
           if (j.le.NTAB) iv(j)=idum
11       continue
         iy=iv(1)
      endif
       k=idum/IQ
          idum=IA*(idum-k*IQ)-IR*k
        if (idum.lt.0) idum=idum+IM
       j=1+iy/NDIV
        iy=iv(j)
        iv(j)=idum
        ran1a=min(AM*iy,RNMX)
      return
     END
```

```
**********************************************************************
*  This subroutine generates a random number according to the        *
*  McIntyre-Conradi distribution for the number of                   *
*  secondary electrons output from an APD in response to one        *
*  primary photoelectron.                                           *
**********************************************************************
c
      FUNCTION mcidev(G,k,idum)
     INTEGER idum
      REAL mcidev,G,k,PI
       PARAMETER (PI=3.141592654)
c
      REAL a0,x0,c0,y,t
      REAL ran1a,pmcint,cmcint
        a0=G/3.0
        x0=-G/50.0
        c0=4.0/G
1          y=a0*tan(PI*ran1a(idum))+x0
       if (y.lt.0.) goto 1
       y=int(y)
          t=pmcint(y,G,k)/cmcint(y,a0,x0,c0)
       if (ran1a(idum).gt.t) goto 1
     mcidev=y
      return
     END
c
c
c The McIntyre distribution
c
       FUNCTION pmcint(y,G,k)
       REAL pmcint,y,G,k
       REAL k1,G1
       DOUBLE PRECISION x1,x2,x3,x4
       INTEGER m,i
c
       k1=1.0-k
       G1=G-1.0
       m=int(y-2.0)
c
       x1=log(  (1+k*G1)/G  )
       x2=1.0+k*y/k1
       x3=log( G1/G )
       x4=0.0
       do 100 i=0, m
100    x4= x4 + log( 1.0+ k*real(i)/( y-real(i) ) )
       pmcint=  exp(  x1*x2+x3*(y-1.0)+x4  )
       return
       end
c
c The comparison function (Lorentzian)
c
       FUNCTION cmcint(x,a0,x0,c0)
       REAL cmcint,x,a0,x0,c0
       cmcint=a0*a0*c0/(   a0*a0+(x-x0)*(x-x0)   )
       return
       end
```

June 7, 1994 webdev.f
X. Sun

```
************************************************************************
*  This subroutine generates a random number according to the      *
*  Webb's distribution for the number of                          *
*  secondary electrons output from an APD in response to n=10     *
*  primary photoelectrons.                                        *
************************************************************************
c
      FUNCTION webdev(nbar,G,F,idum)
     INTEGER idum
      REAL webdev,nbar,G,F,PI
        PARAMETER (PI=3.141592654)
c
      REAL a0,x0,c0,y,t
     REAL ran1a,pwebb,cwebb

         a0=G*sqrt(2.0*F*nbar)
         x0=G*nbar
         c0=1.0/(G*sqrt(F*nbar))
1           y=a0*tan(PI*ran1a(idum))+x0
        if (y.lt.0.) goto 1
        y=int(y)
          t=pwebb(y,nbar,G,F)/cwebb(y,a0,x0,c0)
        if (ran1a(idum).gt.t) goto 1
     webdev=y
      return
    END
c
c
c The Webb distribution
c
        FUNCTION pwebb(y,nbar,G,F)
        REAL pwebb,y,G,F,nbar,PI
        PARAMETER  (PI=3.141592654)
        REAL  x1,x2,x3,x4
c
        x1=2.0*G*G*F*nbar
        x2=y-G*nbar
        x3=1.0+(y-G*nbar)*(F-1.0)/(G*F*nbar)
        x4=1.0/sqrt(PI*x1)/x3/sqrt(x3)
        pwebb=x4*exp(-x2*x2/x1/x3)
        return
        end
c
c The comparison function (Lorentzian)
c
        FUNCTION cwebb(x,a0,x0,c0)
        REAL x,a0,x0,c0,cwebb
        cwebb=a0*a0*c0/(   a0*a0+(x-x0)*(x-x0)   )
        return
        end
```

```
      FUNCTION gasdeva(idum)
      INTEGER idum
      REAL gasdeva
CU    USES ran1a
      INTEGER iset
        REAL fac,gset,rsq,v1,v2,ran1a
      SAVE iset,gset
       DATA iset/0/
       if (iset.eq.0) then
1           v1=2.*ran1a(idum)-1.
           v2=2.*ran1a(idum)-1.
            rsq=v1**2+v2**2
          if(rsq.ge.1..or.rsq.eq.0.)goto 1
            fac=sqrt(-2.*log(rsq)/rsq)
         gset=v1*fac
        gasdeva=v2*fac
        iset=1
      else
       gasdeva=gset
        iset=0
      endif
       return
      END
```

```
      subroutine fltresp(M,fc,Delt,h)
      integer M, k
      real h(M)
      real fc, Delt, hc
c
      do 100 k=1,M
      h(k)=Delt*hc(k*Delt,fc)
100   continue
      return
      end
c
c The continous time impulse response function
c
      function hc(t,fc)
      real hc,t,fc
      integer M1,k
      parameter (M1=5,PI=3.1416)
      complex A(M1), s(M1), chc
c
      A(1)=(0.6163736,1.0986409)
      A(2)=(0.6163736,-1.0986409)
      A(3)=(-4.9168825,-2.6131445)
      A(4)=(-4.9168825,2.6131445)
      A(5)=(8.5950178,0.0)
c
      s(1)=(-0.9576766,1.4711244)
      s(2)=(-0.9576766,-1.4711244)
      s(3)=(-1.3808744,0.7179096)
      s(4)=(-1.3808744,-0.7179096)
      s(5)=(-1.5023160,0.0)
c
      hc=0.0
      do 200 k=1,M1
      chc=A(k)*cexp(  s(k)*2.0*PI*fc*t  )
200   hc=hc+real(chc)
      hc=hc*2.0*PI*fc
      return
      end
```

```
**********************************************************************
*  A subroutine to perform convolution of array 'data' with      *
*  array 'respns'. The dimension of the first array, nd, is      *
*  assumed to be greater than the second, nresp. The resultant   *
*  array is given by 'output'. Zero padding was used when        *
*  calculating the first nresp elements.                         *
**********************************************************************

      subroutine lpfout(data,nd,respns,nresp,output)
      integer nd, nresp, i, j, j0, jj
      real data(nd), respns(nresp), output(nd)

      do 100 i=1,nd
      output(i)=0.0

      if(i.GE.nresp) then
      j0=i-nresp+1
      do 20 j=j0,i
      jj=i-j+1
20    output(i)=output(i)+data(j)*respns(jj)
      else
      do 40 j=1,i
      jj=i-j+1
40    output(i)=output(i)+data(j)*respns(jj)
      end if

100   continue
      return
      end
```